Exploring mechanochemistry of pharmaceutical cocrystals: effect of incident angle on molecular mixing during simulated indentations of two organic solids

Supplementary Information

Michael Ferguson[*a] and Tomislav Friščić[*a]

a) School of Chemistry, University of Birmingham, Edgbaston, Birmingham, B15 2TT, UK

Table of contents

S1 Computational details

S1.1 Molecular dynamics (MD) simulations

The LAMMPS[1] molecular dynamics (MD) engine version 29Oct2020 was utilized to simulate the indentation of a citric acid (**cit**) nanoparticle upon and exposed theophylline (**theo**) surface. The non-reactive OPLS force field parameter set[2] was used to describe the interatomic interactions. Non-bonded interactions were approximated using Lennard-Jones[3] potentials, truncated at 12 Å. Hydrogen bonding interactions were accounted for by incorporating angle-dependent 12-10 form Lennard-Jones potentials, described by the DREIDING[4] force field which are smoothly truncated between 9 Å and 11 Å and is zero for angles lower than 90°. Electrostatic interactions were computed using the particle-particle particle-mesh[5] (PPPM) solver with the accuracy of relative root-mean-square error in per-atom forces set at 1.0×10^5. The partial charges were obtained from *ab initio* methods (see below). Non-bonded and electrostatic interactions for 1-4 pairs were scaled by a factor of 0.5 in accordance with the OPLS force field description.[2] All simulated indentations were carried out in the NVE ensemble with an integration time step of 1 fs.

S1.2 Initial configuration for simulated indentations

The initial configuration for the simulated indentations was formed from two separate systems; (I) a 7×5 supercell of **theo** (3920 molecules, 82,320 atoms) where the (001) surface had been opened by adding 130 Å of vacuum space in the z direction, and (II) and a spherical nanoparticle of **cit** cut from a 12×15 supercell of the bulk crystal (685 molecules, 14,385 atoms) with a final, post-equilibration, radius of 30 Å. The **cit** particle was placed above the xy centre of the **theo** slab with an initial 5 Å separation in z, producing the the system ready for indentations where $\theta = 90°$ (Figure S1).[‡] To control the motion in the indentation, sections molecules of each material were selected to have their velocities fixed throughout the simulations. For **theo**, the 392 molecules that form the bottommost layer of the slab and their velocities were set equal to zero in all three dimensions, ensuring the slab would not experience translational movement as a result of the indentation. For **cit**, the 115 molecules in the uppermost segment of the nanoparticle were selected and their velocities were set the x and z directions to give a total velocity equal to the desired indentation speed (Table S1). All other molecules in the system would have their movement determined through the solution of Newton's laws of motion within LAMMPS. The selections of molecules whose velocities would

---

[‡]All simulation snapshots presented herein were visualised with VMD v1.9.4a55[6] and rendered with Tachyon, v0.99.[7]

be fixed at highlighted in purple in Figure S1. To produced the initial configurations for indentations with θ angles lower than $90°$, the **cit** nanoparticle was negatively displaced in the x direction (Table S2) to ensure that the point of maximum indentations was equal for all trajectories.
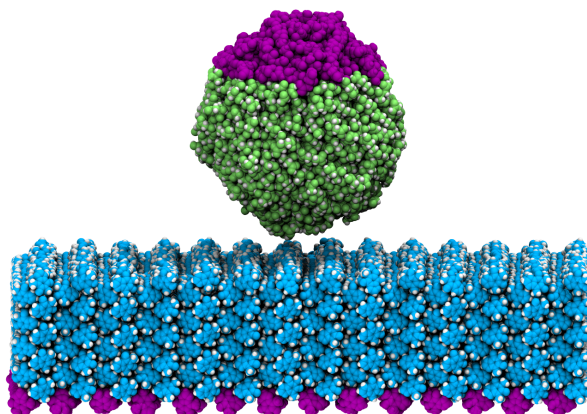
Figure S1 Snapshot of the initial configurations for simulated indentations of **cit** nanoparticle (green) upon a slab of **theo** (blue) with the (001) surface exposed with an incident angle of $90°$. Purple regions highlight molecules whose trajectories are fixed throughout the simulation to effectuate the desired indentation. Hydrogen atoms are rendered in white for aesthetic purposes.

Table S1 Components of velocities in the x and z directions applied to 115 molecules of **cit** to perform indentations for a range of total indentation speeds ($16\,\mathrm{m\,s^{-1}}$ to $1\,\mathrm{m\,s^{-1}}$) and angles ($\theta = 90°$ to $15°$).

θ / $°$	Nanoparticle speed / $\times 10^{-5}$ Å·fs^{-1}							
	16		8		4		1	
	x	z	x	z	x	z	x	z
15	15.455	-4.141	7.727	-2.071	3.864	-1.035	0.966	-0.259
30	13.856	-8.000	6.928	-4.000	3.464	-2.000	0.866	-0.500
45	11.314	-11.314	5.657	-5.657	2.828	-2.828	0.707	-0.707
60	8.000	-13.856	4.000	-6.928	2.000	-3.464	0.500	-0.866
75	4.141	-15.455	2.071	-7.727	1.035	-3.864	0.259	-0.966
90	0.000	-16.00	0.000	-8.000	0.000	-4.000	0.000	-1.000

Table S2 Displacements applied to the **cit** nanoparticle in the x direction to ensure that all simulations have the same point of maximum indentation.

θ / $°$	90	75	60	45	30	15
$\Delta x_{(\boldsymbol{cit})}$ / Å	0.0000	-6.6987	-14.4338	25.0000	-43.3013	-93.3013

S1.3   Periodic density functional theory (DFT) calculations

DFT was employed to obtain partial atomic charges for all atoms of citric acid and theophylline. We used the plane wave code CASTEP,[8] (v22.11) to perform the calculations. Input structures for **cit** and **theo** were obtained from the Cambridge structural database[9] (CSD) with the reference codes, CITRAC10,[10] and BAPLOT01,[11] respectively. Input files for CASTEP were then generated using the cif2cell program.[12] The structures were optimised using the PBE functional[13] with the Grimme-D3 dispersion correction applied.[14] The cut off energy of the plane wave basis was set at $900\,\mathrm{eV}$ with core regions of electron density described by on-the-fly ultrasoft psuedopotentials from the CASTEP library. Brillouin zone sampling was performed using Monkhorst-Pack grids with a $\boldsymbol{k}$-point spacing of $0.07\ 2\pi$ Å^{-1} The convergence criteria for the geometry optimisations were; energy $= 2 \times 10^{-5}\,\mathrm{eV}$, force $= 5 \times 10^{-2}\,\mathrm{eV\,atom^{-1}}$,

stress = 0.1 GPa, and displacement = 2×10^{-3} Å. Upon convergence a Hirshfeld analysis[15] was performed to obtain the partial charges for each atom in the structure.
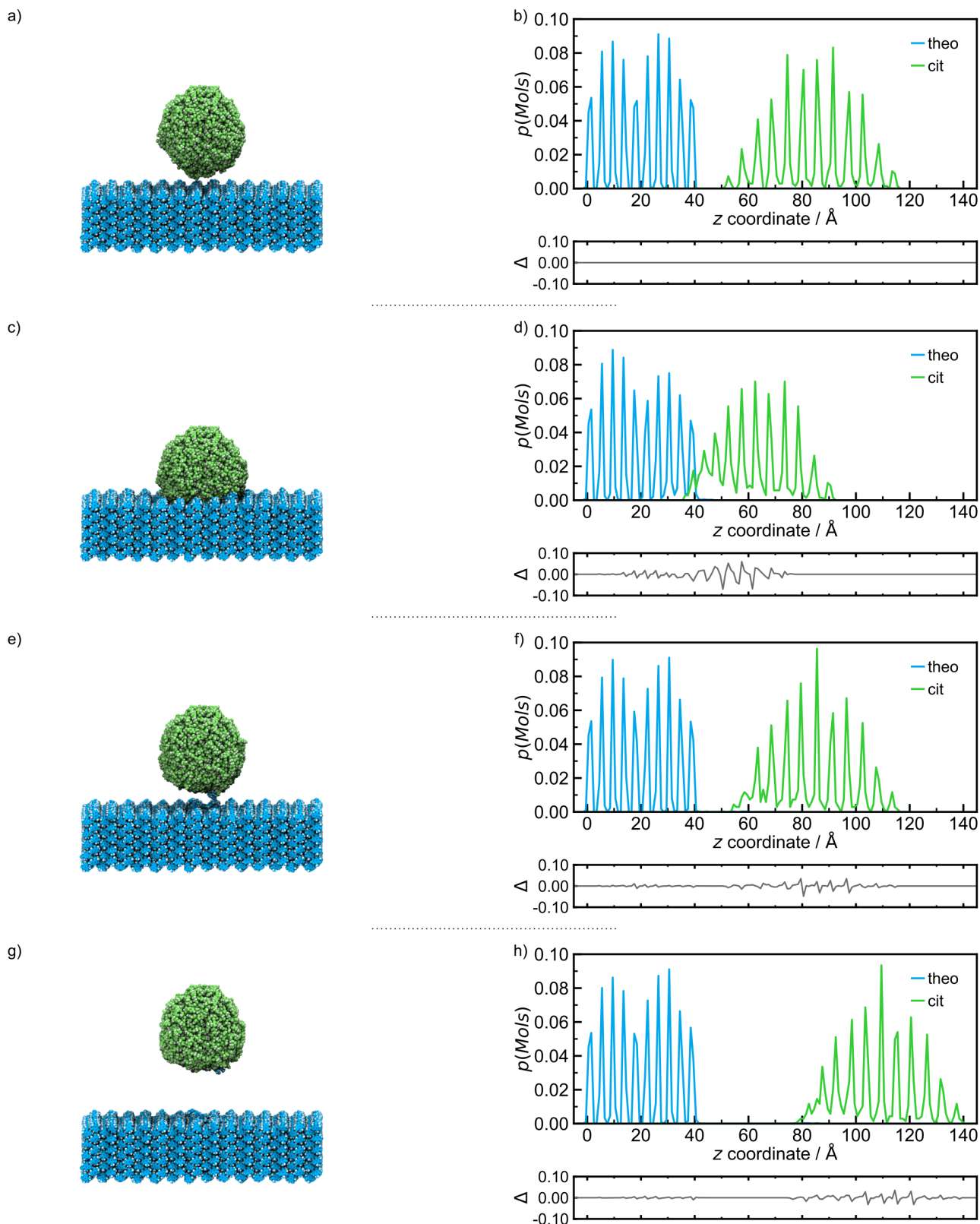
S2 Molecular transfer analysis

To study the molecular transfer that occurred between **cit** and **theo** we monitored the positions of molecules along the z direction. Firstly, the centre of mass (COM) of every molecule in the system was determined. Then a probability density histogram was created for each species separately from the z components of the COM data for each frame in a given trajectory. Species were treated separately at this stage to account for the large difference in the number of molecules of **theo** (3920) and **cit** (685). The z components of the COM data were collected into 150 bins with a bin width equal to 1 Å. This range was selected as the maximum separation in z of any molecule of **cit** from the bottom of the **theo** slab never exceeded 145 Å. Using the final frame of data, the total number of molecules transferred was obtained by determining the number of **theo** molecules whose COM z coordinate was greater than 55 Å and the number of **cit** molecules whose COM z coordinate was lesser than 55 Å. Using the initial configuration as the reference point a difference curve is given under each distribution which highlights the between each stage of the simulation. In each case the reference distribution for **cit** was shifted in z to correctly align the section corresponding to the particles with fixed trajectories before the subtraction was performed. The molecular transfer analysis was performed using a script written in Python3 [16] with the NumPy [17] and matplotlib [18] libraries used to generate the histograms and plots, respectively. The percentage number of free-to-move molecules transferred during the simulated indentations are given in Table S3 below.

Table S3 Percentage number of free-to-move molecules transferred between **cit** and **theo** for simulated indentations over a range of indentation speeds (16 m s^{-1} to 1 m s^{-1}) and angles ($\theta = 90°$ to $15°$).
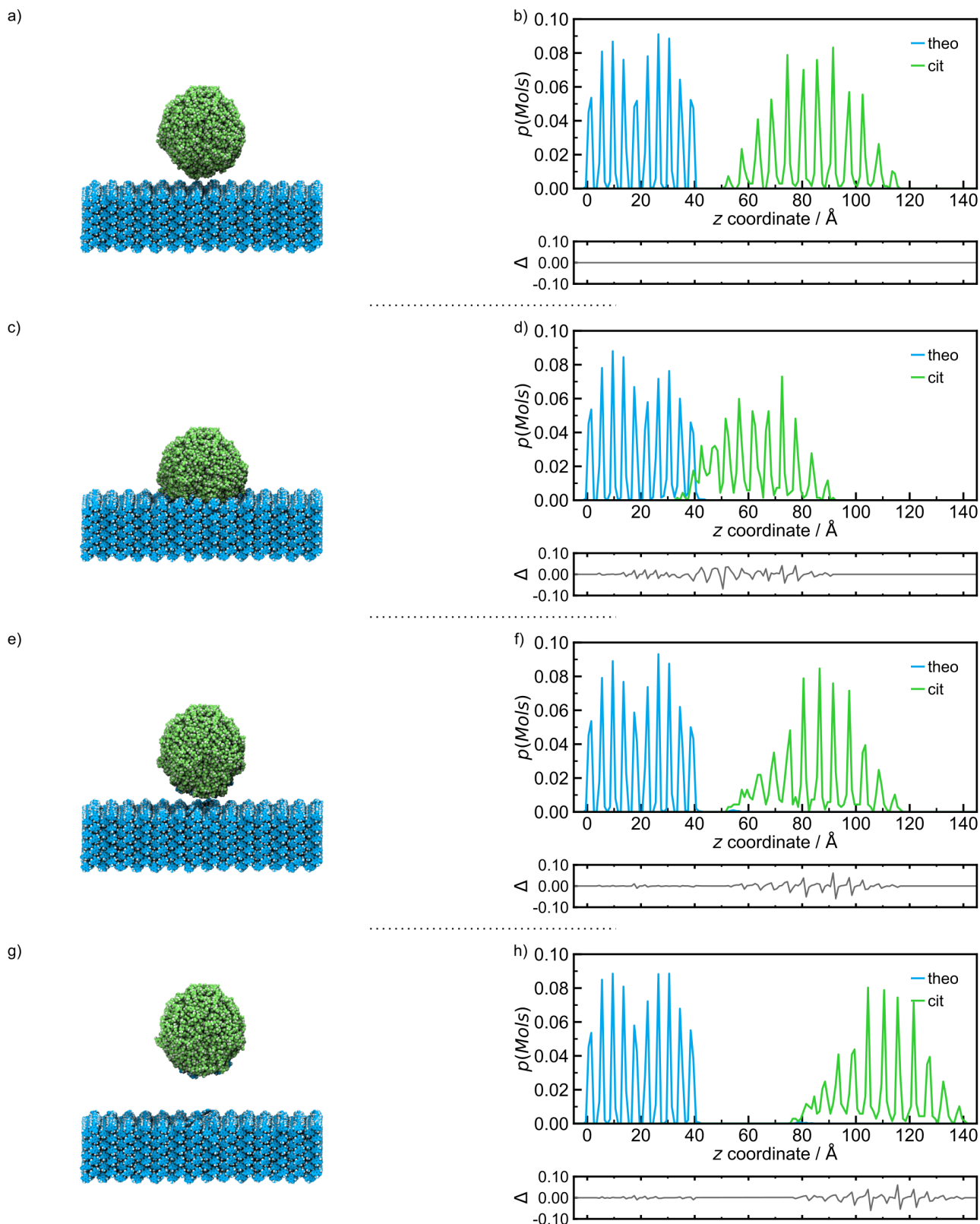
v / m s^{-1}	θ / $°$					
	90	75	60	45	30	15
	Percentage of molecules transferred / %					
16	0.15	0.20	0.22	0.07	0.29	0.68
8	0.32	0.07	0.17	0.29	0.44	1.10
4	0.12	0.02	0.22	0.20	0.34	0.29
1	0.10	0.20	0.12	0.07	0.10	1.29

Indentation parameters: $\theta = 90°$, **Indentation speed** $16\,\text{m}\,\text{s}^{-1}$
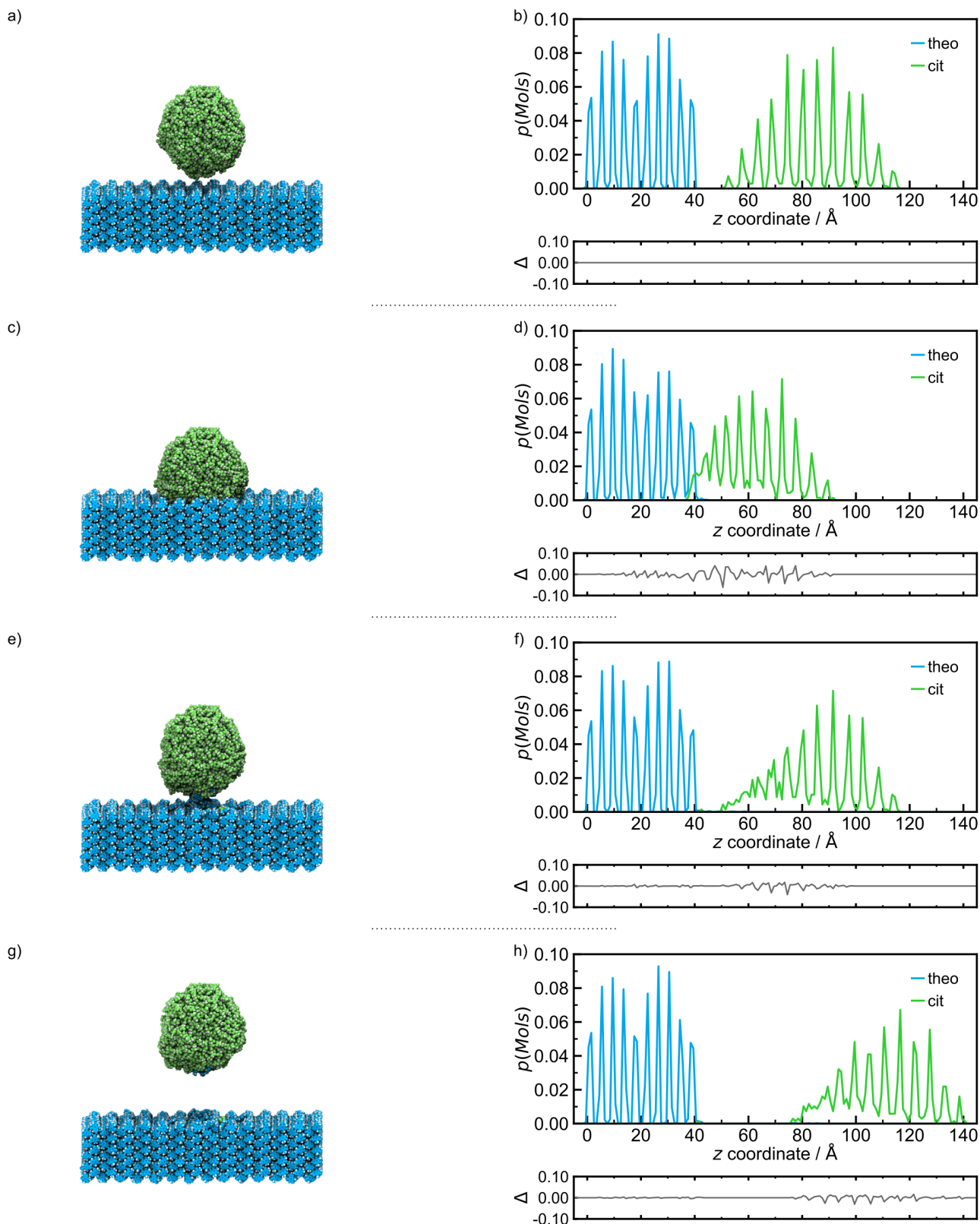

Figure S2 Left: Snapshots of the indentation of **cit** nanoparticle (green) upon the (001) slab of **theo** (blue) where the nanoparticle travels at $16\,\text{m}\,\text{s}^{-1}$ and an incident angle of $90°$. The snapshots show a) the initial configuration, c) the point of maximum indentation, e) after retraction of $25\,\text{Å}$, and g) the final configuration after retraction of $50\,\text{Å}$. Hydrogen atoms are rendered in white for aesthetic purposes. Right: Distribution of molecules, as a percentage of the species, of **theo** (blue) and **cit** (green) for b) the initial configuration, d) the point of maximum indentation, f) after $25\,\text{Å}$ retraction, and h) the final configuration.

Indentation parameters: $\theta = 90°$, **Indentation speed** $8\,\text{m}\,\text{s}^{-1}$
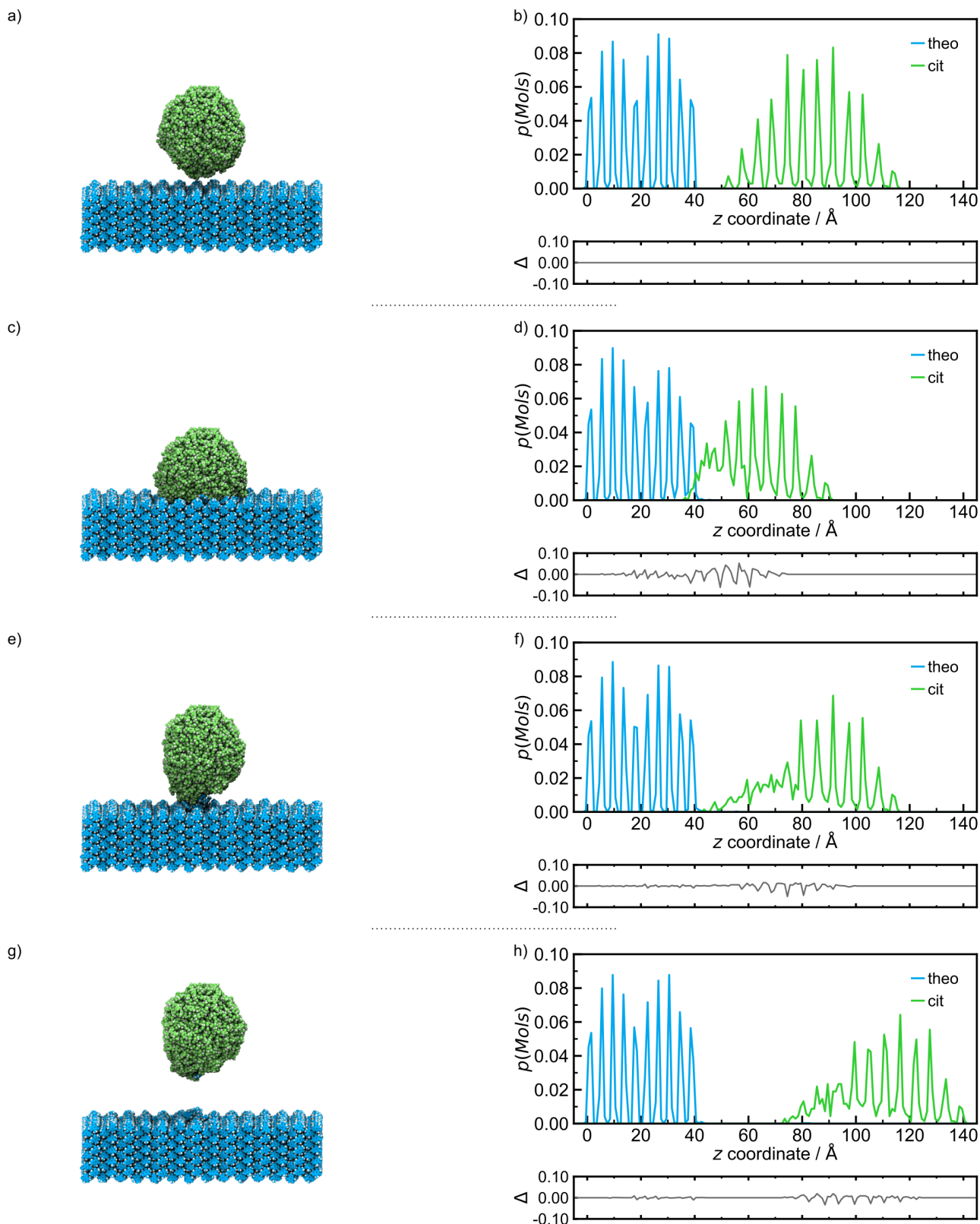

Figure S3 Left: Snapshots of the indentation of **cit** nanoparticle (green) upon the (001) slab of **theo** (blue) where the nanoparticle travels at $8\,\text{m}\,\text{s}^{-1}$ and an incident angle of $90°$. The snapshots show a) the initial configuration, c) the point of maximum indentation, e) after retraction of $25\,\text{Å}$, and g) the final configuration after retraction of $50\,\text{Å}$. Hydrogen atoms are rendered in white for aesthetic purposes. Right: Distribution of molecules, as a percentage of the species, of **theo** (blue) and **cit** (green) for b) the initial configuration, d) the point of maximum indentation, f) after $25\,\text{Å}$ retraction, and h) the final configuration.

Indentation parameters: $\theta = 90°$, **Indentation speed** $4\,\mathrm{m\,s^{-1}}$

Figure S4 Left: Snapshots of the indentation of **cit** nanoparticle (green) upon the (001) slab of **theo** (blue) where the nanoparticle travels at $4\,\mathrm{m\,s^{-1}}$ and an incident angle of $90°$. The snapshots show a) the initial configuration, c) the point of maximum indentation, e) after retraction of $25\,\text{Å}$, and g) the final configuration after retraction of $50\,\text{Å}$. Hydrogen atoms are rendered in white for aesthetic purposes. Right: Distribution of molecules, as a percentage of the species, of **theo** (blue) and **cit** (green) for b) the initial configuration, d) the point of maximum indentation, f) after $25\,\text{Å}$ retraction, and h) the final configuration.
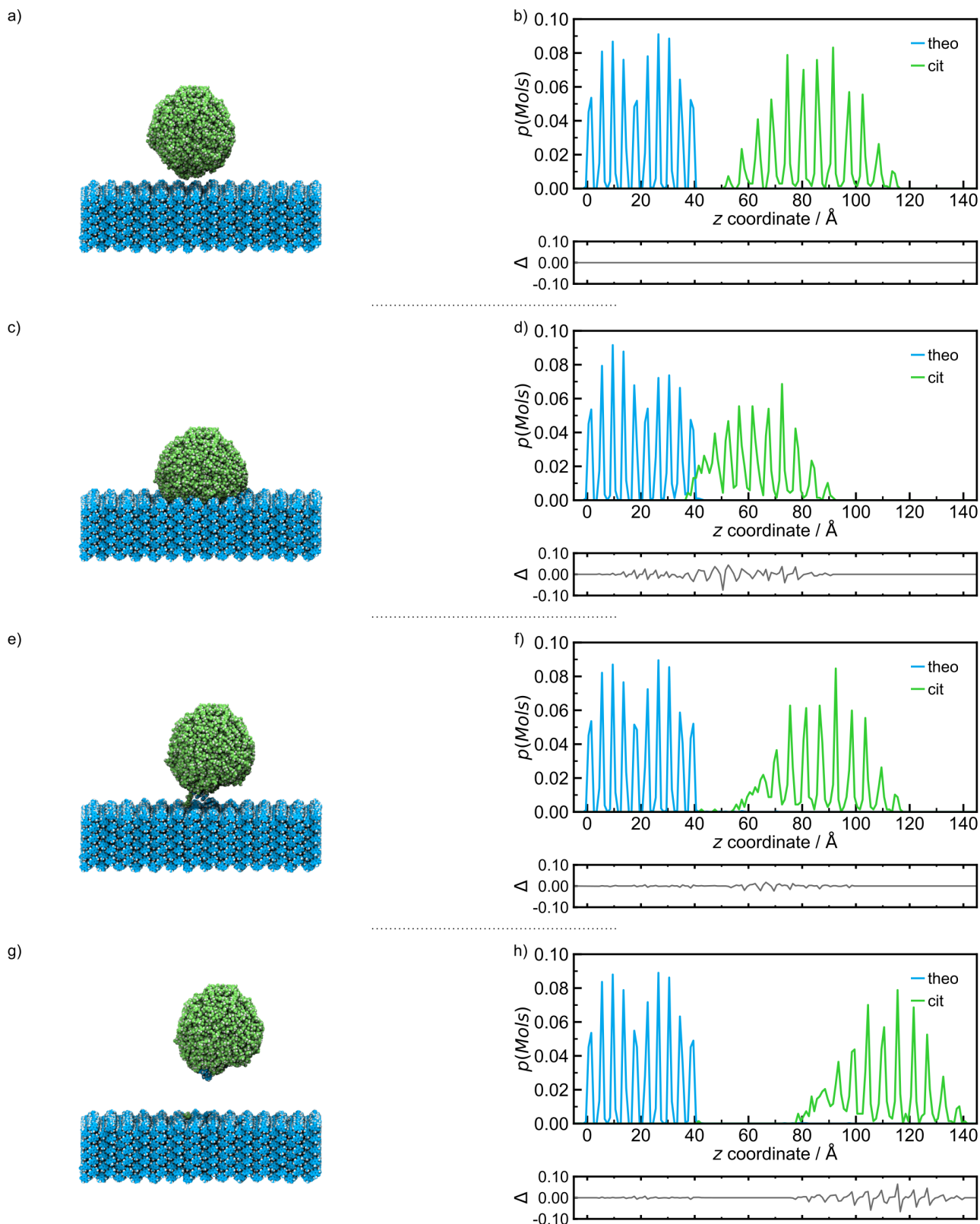
Indentation parameters: $\theta = 90°$, **Indentation speed** $1\,\mathrm{m\,s^{-1}}$

Figure S5 Left: Snapshots of the indentation of **cit** nanoparticle (green) upon the (001) slab of **theo** (blue) where the nanoparticle travels at $1\,\mathrm{m\,s^{-1}}$ and an incident angle of $90°$. The snapshots show a) the initial configuration, c) the point of maximum indentation, e) after retraction of $25\,\mathrm{\AA}$, and g) the final configuration after retraction of $50\,\mathrm{\AA}$. Hydrogen atoms are rendered in white for aesthetic purposes. Right: Distribution of molecules, as a percentage of the species, of **theo** (blue) and **cit** (green) for b) the initial configuration, d) the point of maximum indentation, f) after $25\,\mathrm{\AA}$ retraction, and h) the final configuration.
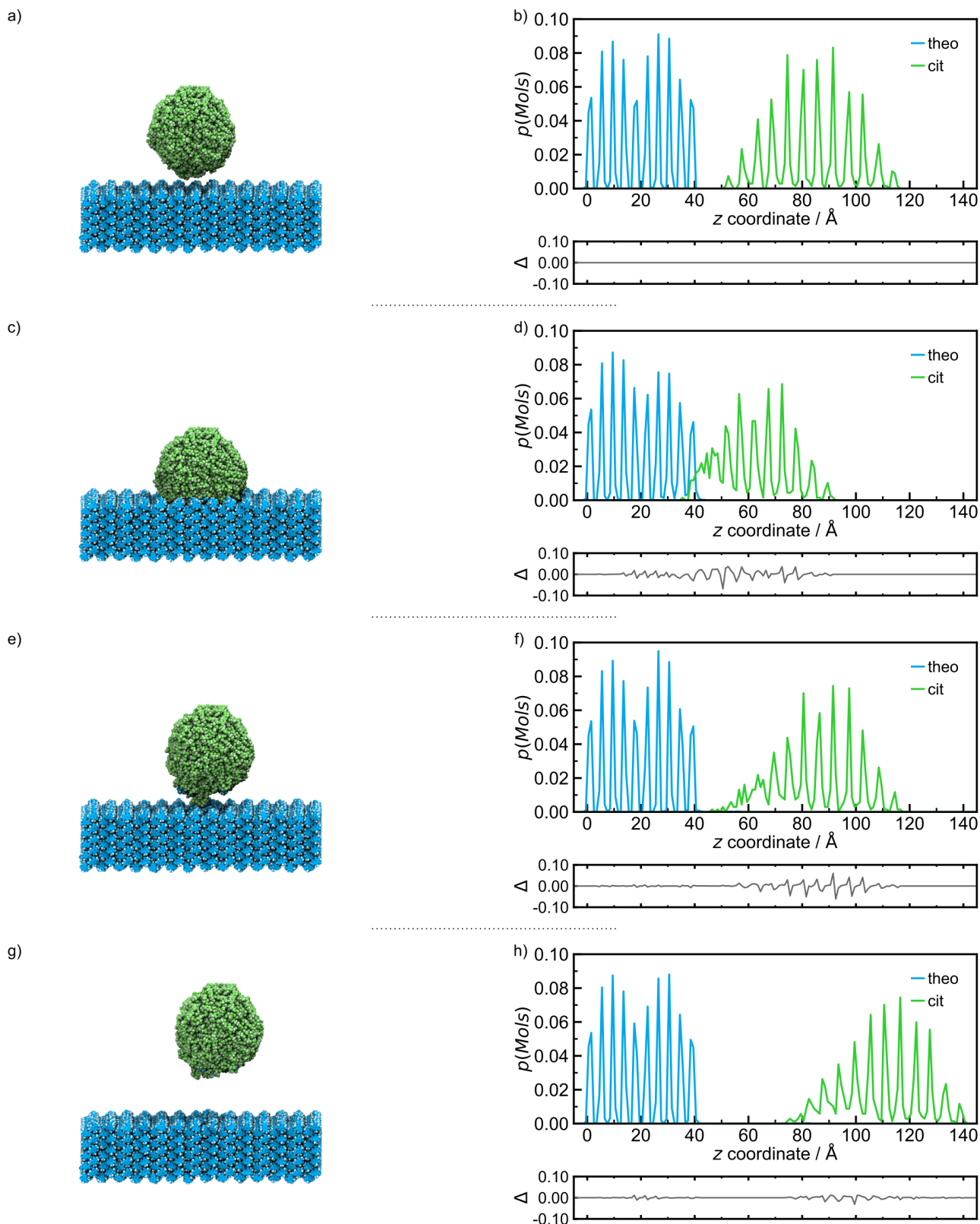
Indentation parameters: $\theta = 75°$, **Indentation speed** $16\,\mathrm{m\,s^{-1}}$

Figure S6 Left: Snapshots of the indentation of **cit** nanoparticle (green) upon the (001) slab of **theo** (blue) where the nanoparticle travels at $16\,\mathrm{m\,s^{-1}}$ and an incident angle of $75°$. The snapshots show a) the initial configuration, c) the point of maximum indentation, e) after retraction of $25\,\text{Å}$, and g) the final configuration after retraction of $50\,\text{Å}$. Hydrogen atoms are rendered in white for aesthetic purposes. Right: Distribution of molecules, as a percentage of the species, of **theo** (blue) and **cit** (green) for b) the initial configuration, d) the point of maximum indentation, f) after $25\,\text{Å}$ retraction, and h) the final configuration.
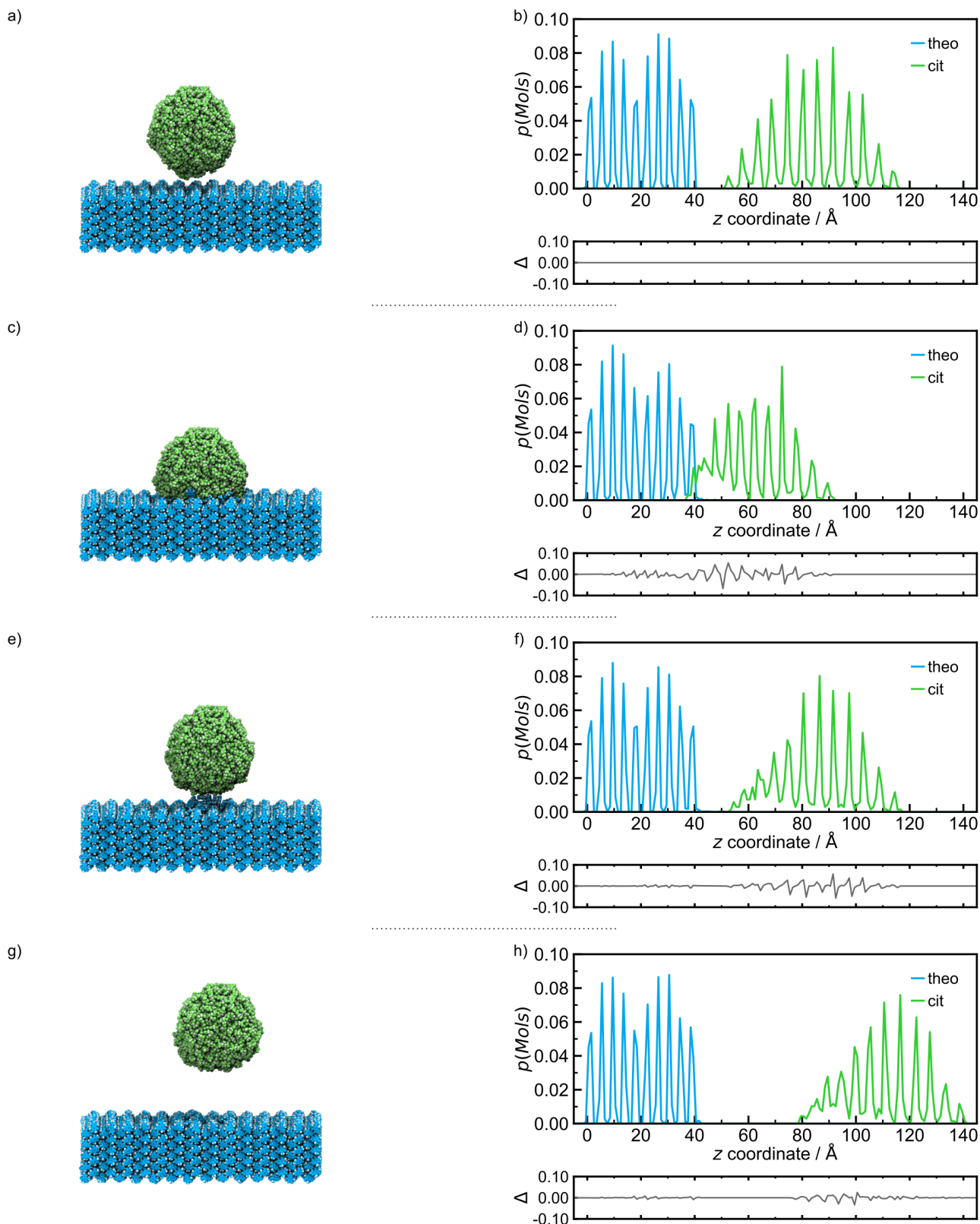
Indentation parameters: $\theta = 75°$, **Indentation speed** $8\,\mathrm{m\,s^{-1}}$

Figure S7 Left: Snapshots of the indentation of **cit** nanoparticle (green) upon the (001) slab of **theo** (blue) where the nanoparticle travels at $8\,\mathrm{m\,s^{-1}}$ and an incident angle of $75°$. The snapshots show a) the initial configuration, c) the point of maximum indentation, e) after retraction of $25\,\text{Å}$, and g) the final configuration after retraction of $50\,\text{Å}$. Hydrogen atoms are rendered in white for aesthetic purposes. Right: Distribution of molecules, as a percentage of the species, of **theo** (blue) and **cit** (green) for b) the initial configuration, d) the point of maximum indentation, f) after $25\,\text{Å}$ retraction, and h) the final configuration.

Indentation parameters: $\theta = 75°$, **Indentation speed** $4\,\mathrm{m\,s^{-1}}$

Figure S8 Left: Snapshots of the indentation of **cit** nanoparticle (green) upon the (001) slab of **theo** (blue) where the nanoparticle travels at $4\,\mathrm{m\,s^{-1}}$ and an incident angle of 75°. The snapshots show a) the initial configuration, c) the point of maximum indentation, e) after retraction of 25 Å, and g) the final configuration after retraction of 50 Å. Hydrogen atoms are rendered in white for aesthetic purposes. Right: Distribution of molecules, as a percentage of the species, of **theo** (blue) and **cit** (green) for b) the initial configuration, d) the point of maximum indentation, f) after 25 Å retraction, and h) the final configuration.
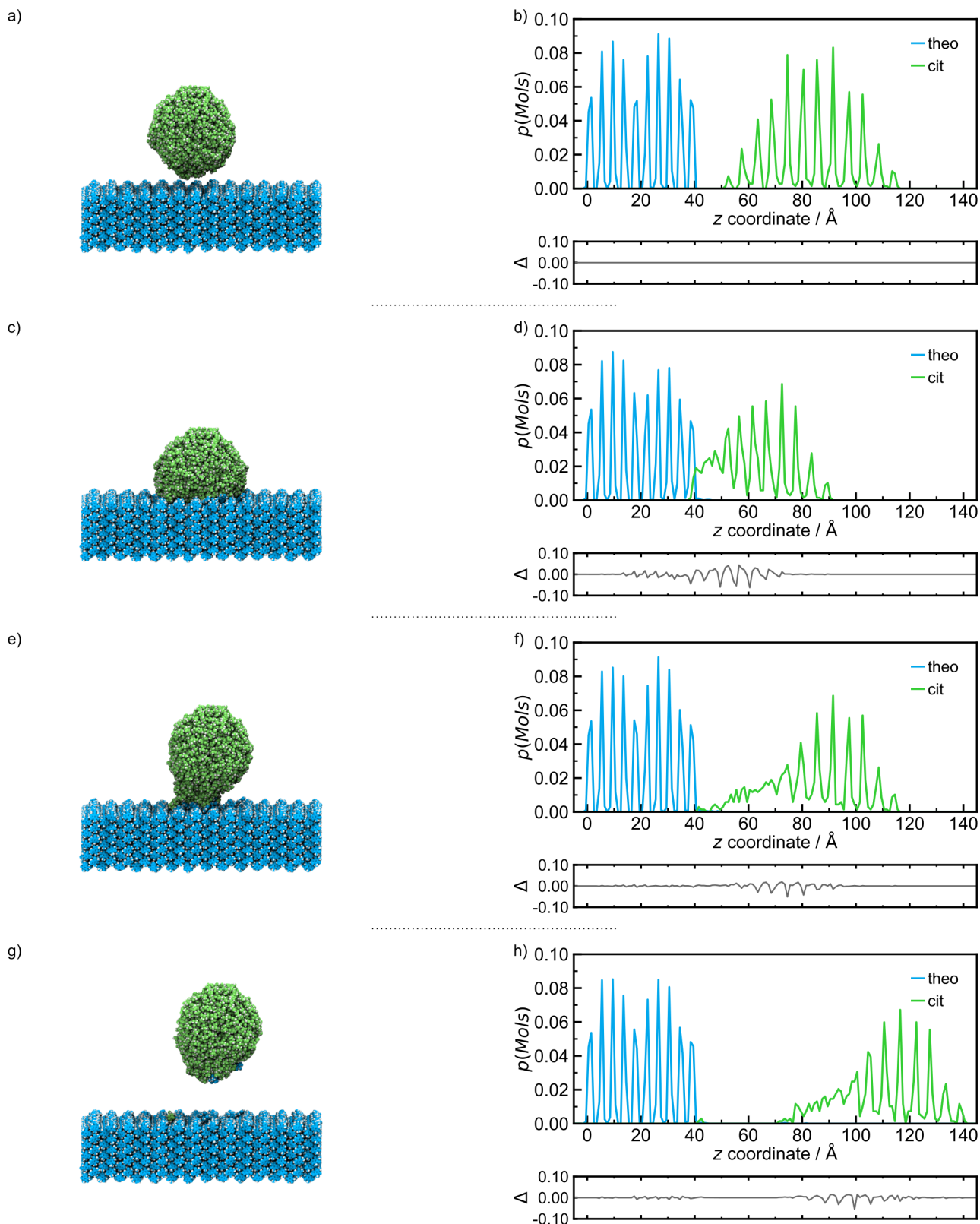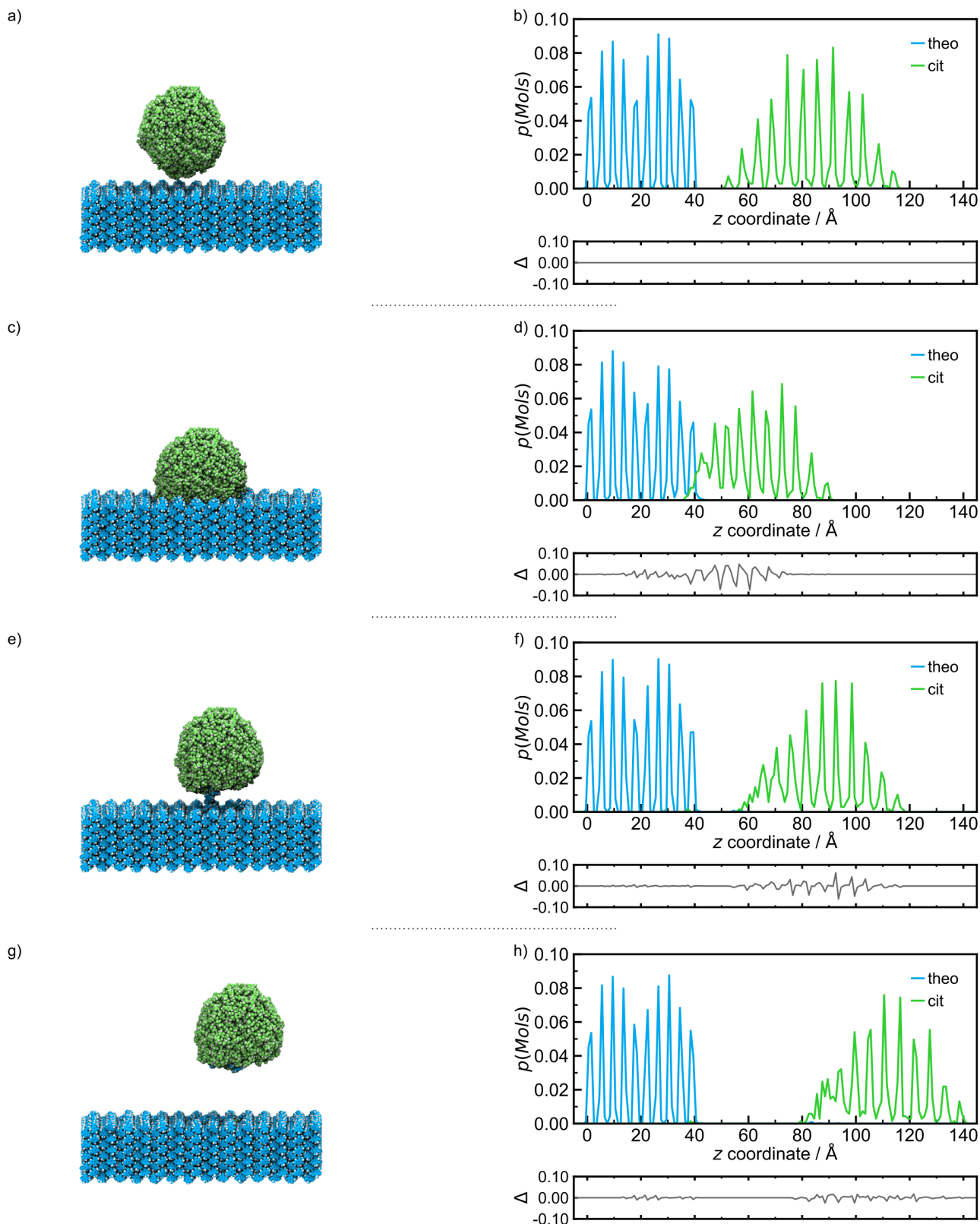
Indentation parameters: $\theta = 75°$, **Indentation speed** $1\,\mathrm{m\,s^{-1}}$
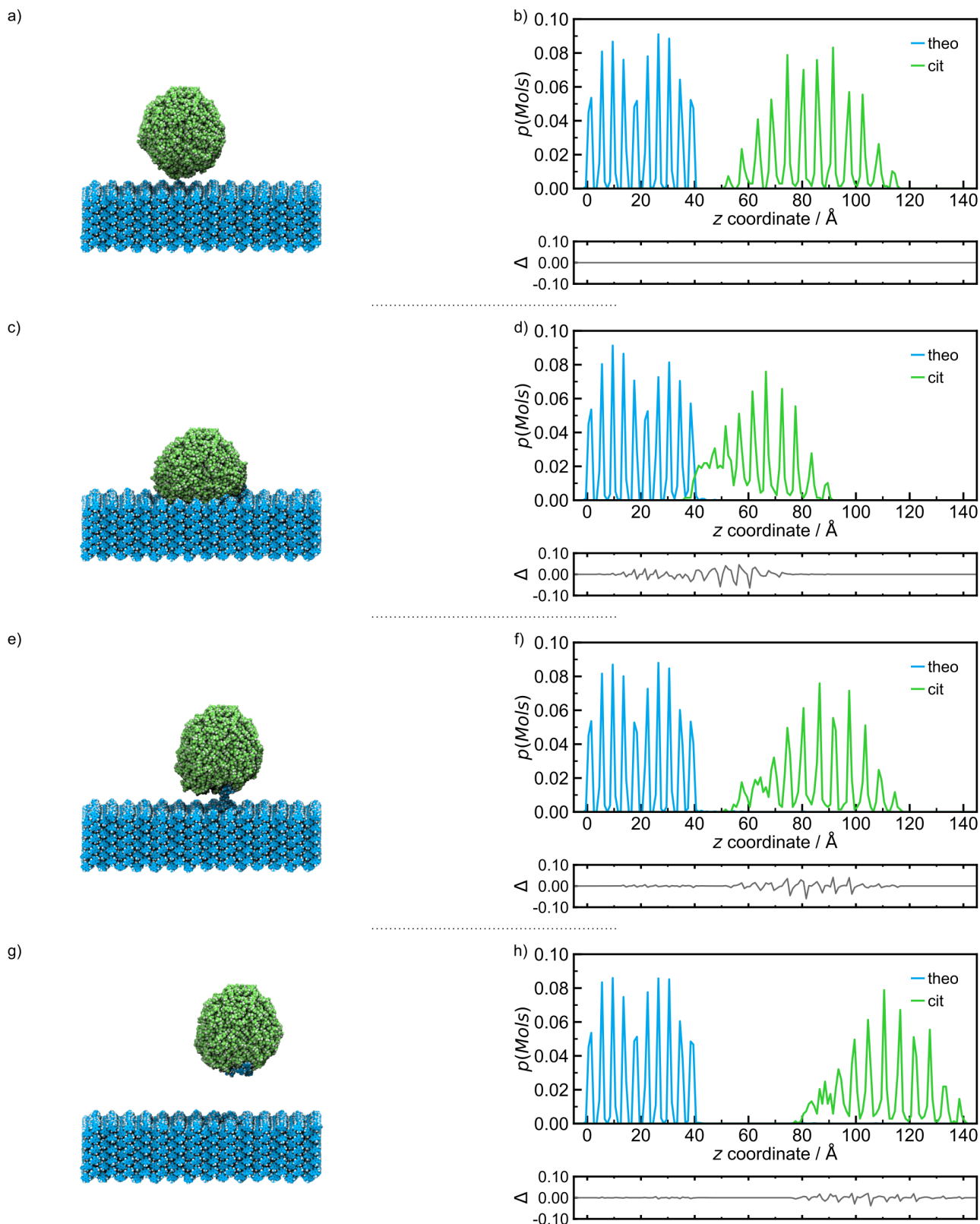

Figure S9 Left: Snapshots of the indentation of **cit** nanoparticle (green) upon the (001) slab of **theo** (blue) where the nanoparticle travels at $1\,\mathrm{m\,s^{-1}}$ and an incident angle of $75°$. The snapshots show a) the initial configuration, c) the point of maximum indentation, e) after retraction of $25\,\text{Å}$, and g) the final configuration after retraction of $50\,\text{Å}$. Hydrogen atoms are rendered in white for aesthetic purposes. Right: Distribution of molecules, as a percentage of the species, of **theo** (blue) and **cit** (green) for b) the initial configuration, d) the point of maximum indentation, f) after $25\,\text{Å}$ retraction, and h) the final configuration.

Indentation parameters: $\theta = 60°$, **Indentation speed** $16\,\mathrm{m\,s^{-1}}$

Figure S10 Left: Snapshots of the indentation of **cit** nanoparticle (green) upon the (001) slab of **theo** (blue) where the nanoparticle travels at $16\,\mathrm{m\,s^{-1}}$ and an incident angle of $60°$. The snapshots show a) the initial configuration, c) the point of maximum indentation, e) after retraction of $25\,\text{Å}$, and g) the final configuration after retraction of $50\,\text{Å}$. Hydrogen atoms are rendered in white for aesthetic purposes. Right: Distribution of molecules, as a percentage of the species, of **theo** (blue) and **cit** (green) for b) the initial configuration, d) the point of maximum indentation, f) after $25\,\text{Å}$ retraction, and h) the final configuration.

Indentation parameters: $\theta = 60°$, **Indentation speed** $8\,\mathrm{m\,s^{-1}}$

Figure S11 Left: Snapshots of the indentation of **cit** nanoparticle (green) upon the (001) slab of **theo** (blue) where the nanoparticle travels at $8\,\mathrm{m\,s^{-1}}$ and an incident angle of $60°$. The snapshots show a) the initial configuration, c) the point of maximum indentation, e) after retraction of $25\,\text{Å}$, and g) the final configuration after retraction of $50\,\text{Å}$. Hydrogen atoms are rendered in white for aesthetic purposes. Right: Distribution of molecules, as a percentage of the species, of **theo** (blue) and **cit** (green) for b) the initial configuration, d) the point of maximum indentation, f) after $25\,\text{Å}$ retraction, and h) the final configuration.
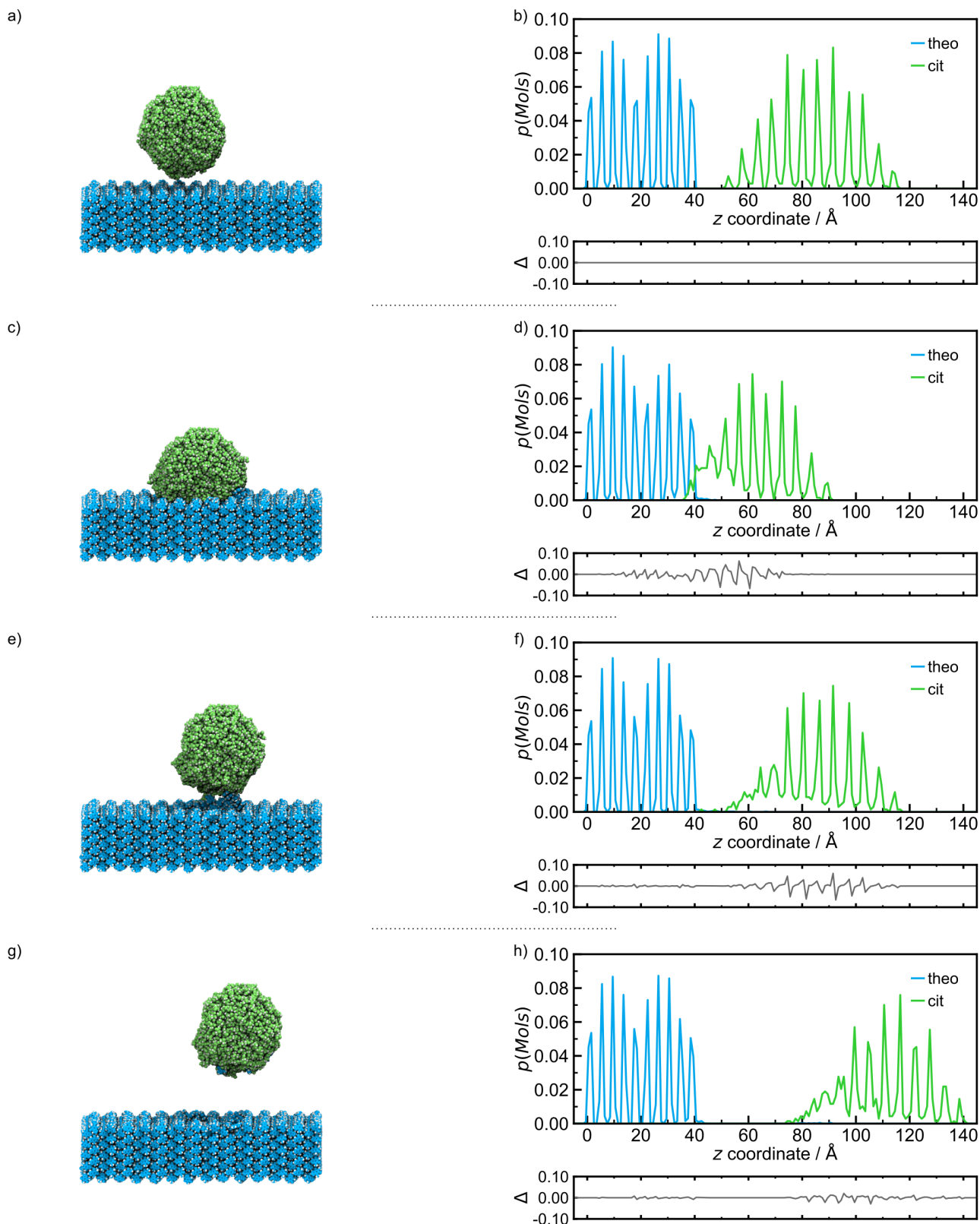
Indentation parameters: $\theta = 60°$, **Indentation speed** $4\,\mathrm{m\,s^{-1}}$

Figure S12 Left: Snapshots of the indentation of **cit** nanoparticle (green) upon the (001) slab of **theo** (blue) where the nanoparticle travels at $4\,\mathrm{m\,s^{-1}}$ and an incident angle of $60°$. The snapshots show a) the initial configuration, c) the point of maximum indentation, e) after retraction of $25\,\text{Å}$, and g) the final configuration after retraction of $50\,\text{Å}$. Hydrogen atoms are rendered in white for aesthetic purposes. Right: Distribution of molecules, as a percentage of the species, of **theo** (blue) and **cit** (green) for b) the initial configuration, d) the point of maximum indentation, f) after $25\,\text{Å}$ retraction, and h) the final configuration.
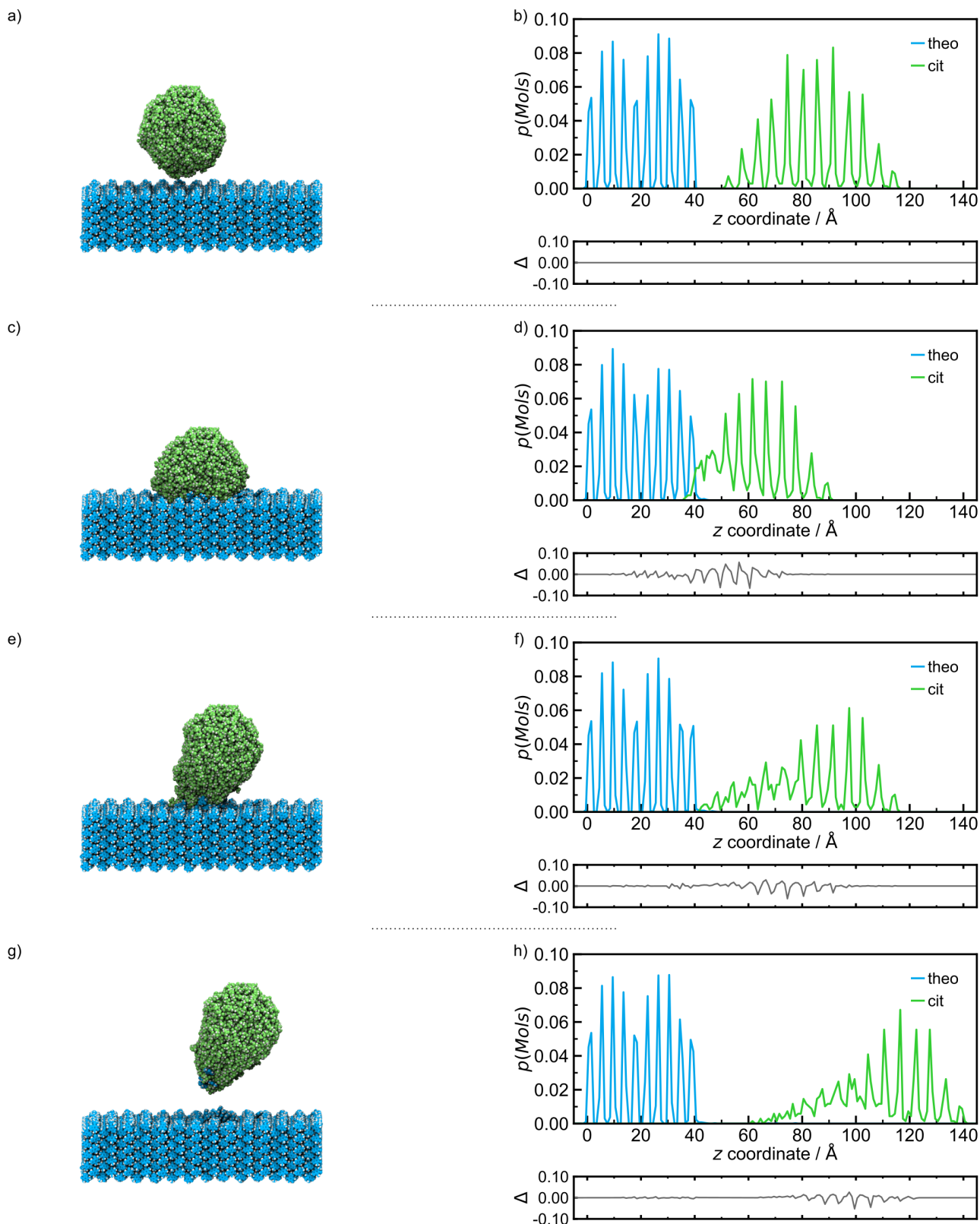
Indentation parameters: $\theta = 60°$, **Indentation speed** $1\,\mathrm{m\,s^{-1}}$
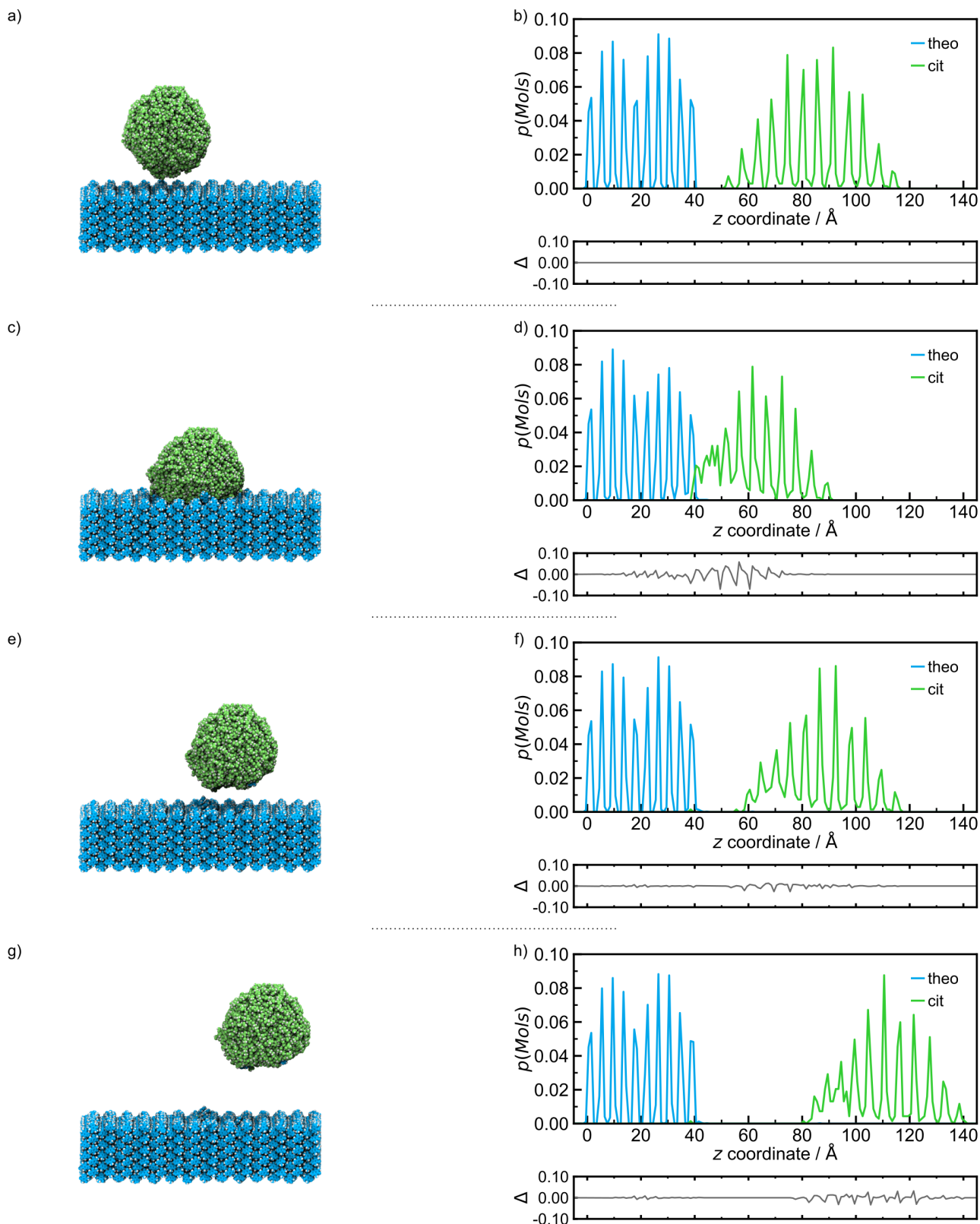

Figure S13 Left: Snapshots of the indentation of **cit** nanoparticle (green) upon the (001) slab of **theo** (blue) where the nanoparticle travels at $1\,\mathrm{m\,s^{-1}}$ and an incident angle of $60°$. The snapshots show a) the initial configuration, c) the point of maximum indentation, e) after retraction of $25\,\text{Å}$, and g) the final configuration after retraction of $50\,\text{Å}$. Hydrogen atoms are rendered in white for aesthetic purposes. Right: Distribution of molecules, as a percentage of the species, of **theo** (blue) and **cit** (green) for b) the initial configuration, d) the point of maximum indentation, f) after $25\,\text{Å}$ retraction, and h) the final configuration.

Indentation parameters: $\theta = 45°$, **Indentation speed** $16\,\mathrm{m\,s^{-1}}$
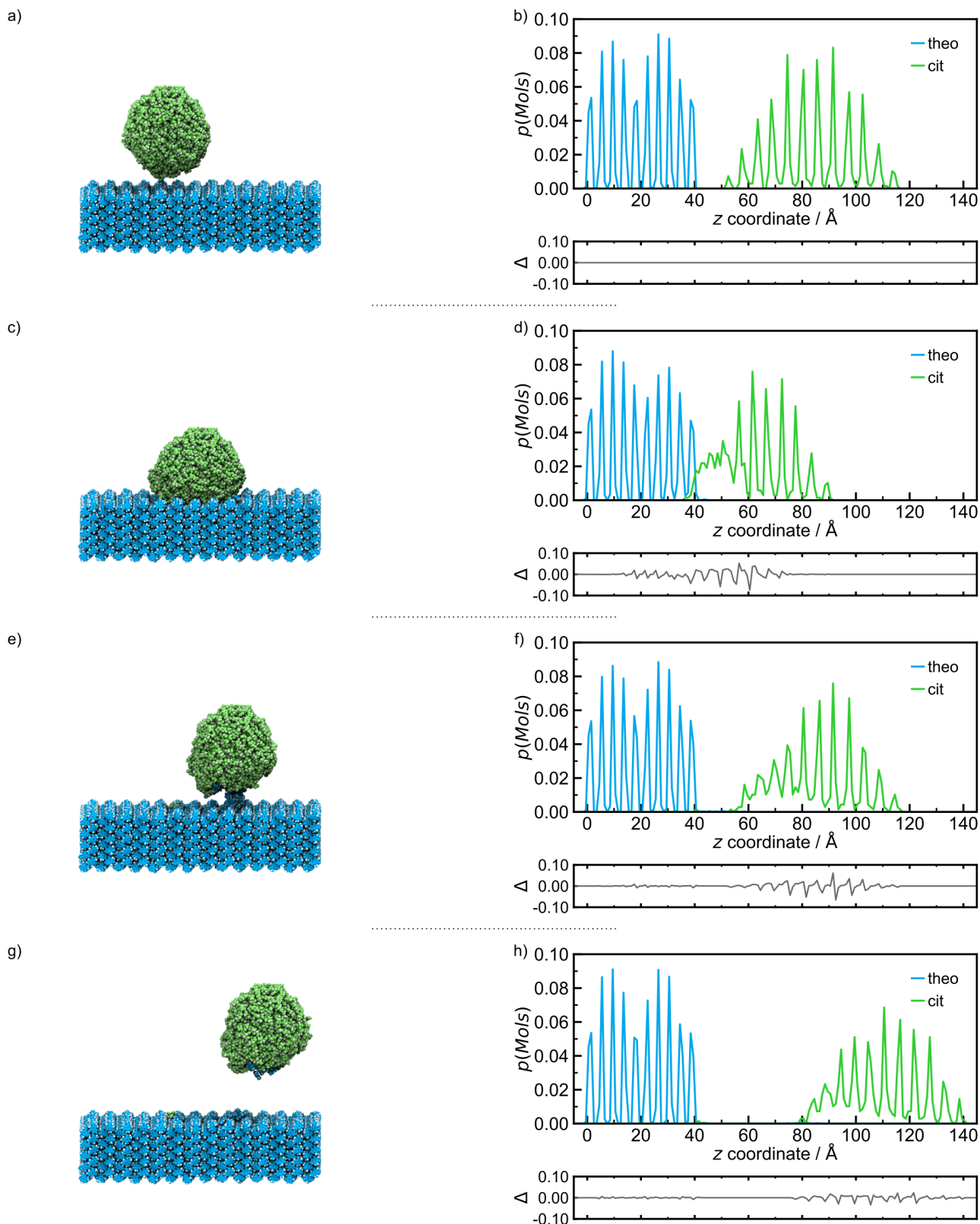

Figure S14 Left: Snapshots of the indentation of **cit** nanoparticle (green) upon the (001) slab of **theo** (blue) where the nanoparticle travels at $16\,\mathrm{m\,s^{-1}}$ and an incident angle of $45°$. The snapshots show a) the initial configuration, c) the point of maximum indentation, e) after retraction of $25\,\text{Å}$, and g) the final configuration after retraction of $50\,\text{Å}$. Hydrogen atoms are rendered in white for aesthetic purposes. Right: Distribution of molecules, as a percentage of the species, of **theo** (blue) and **cit** (green) for b) the initial configuration, d) the point of maximum indentation, f) after $25\,\text{Å}$ retraction, and h) the final configuration.

Indentation parameters: $\theta = 45°$, **Indentation speed** $8\,\mathrm{m\,s^{-1}}$

Figure S15 Left: Snapshots of the indentation of **cit** nanoparticle (green) upon the (001) slab of **theo** (blue) where the nanoparticle travels at $8\,\mathrm{m\,s^{-1}}$ and an incident angle of $45°$. The snapshots show a) the initial configuration, c) the point of maximum indentation, e) after retraction of $25\,\text{Å}$, and g) the final configuration after retraction of $50\,\text{Å}$. Hydrogen atoms are rendered in white for aesthetic purposes. Right: Distribution of molecules, as a percentage of the species, of **theo** (blue) and **cit** (green) for b) the initial configuration, d) the point of maximum indentation, f) after $25\,\text{Å}$ retraction, and h) the final configuration.
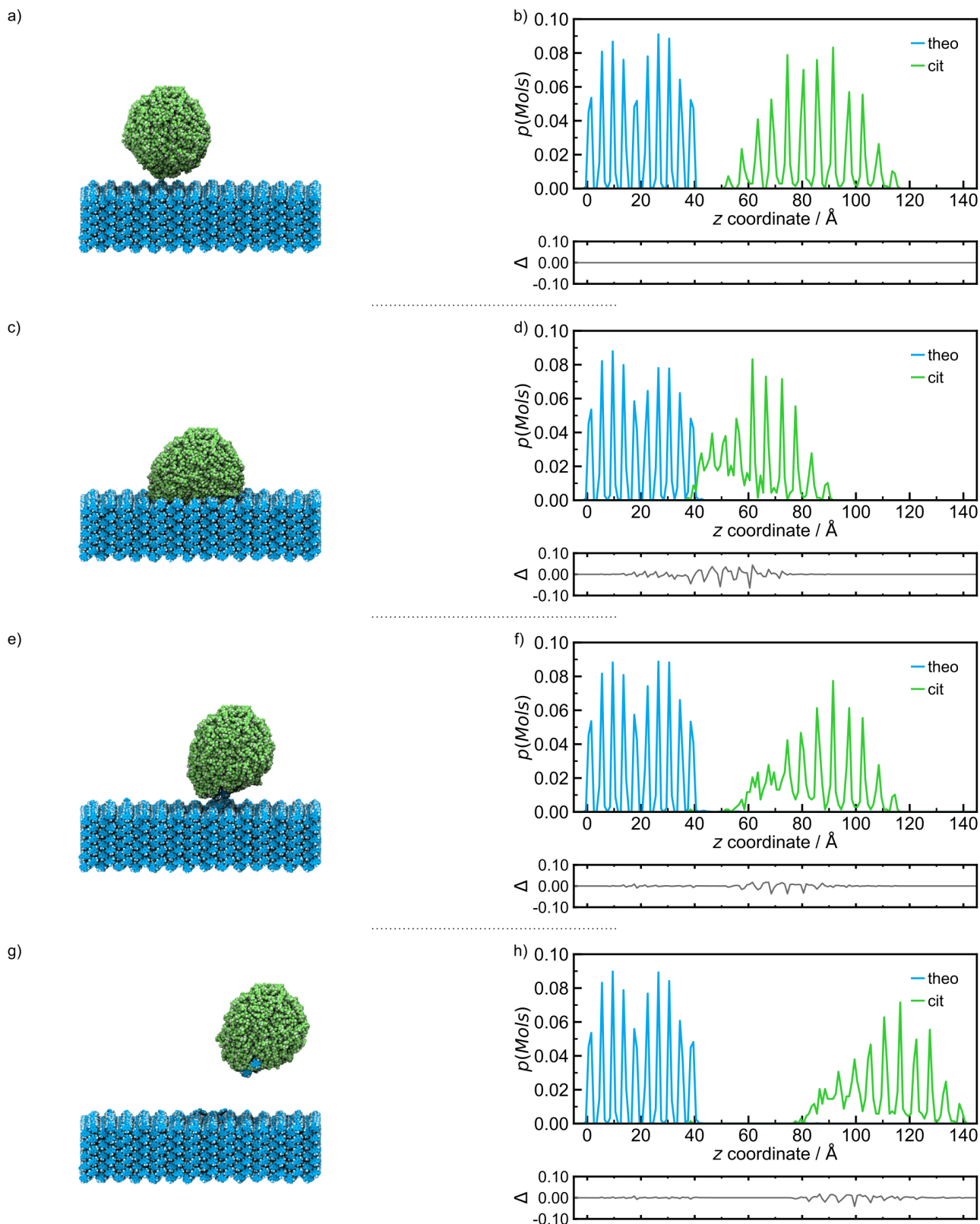
Indentation parameters: $\theta = 45°$, **Indentation speed** $4\,\mathrm{m\,s^{-1}}$

Figure S16 Left: Snapshots of the indentation of **cit** nanoparticle (green) upon the (001) slab of **theo** (blue) where the nanoparticle travels at $4\,\mathrm{m\,s^{-1}}$ and an incident angle of $45°$. The snapshots show a) the initial configuration, c) the point of maximum indentation, e) after retraction of $25\,\text{Å}$, and g) the final configuration after retraction of $50\,\text{Å}$. Hydrogen atoms are rendered in white for aesthetic purposes. Right: Distribution of molecules, as a percentage of the species, of **theo** (blue) and **cit** (green) for b) the initial configuration, d) the point of maximum indentation, f) after $25\,\text{Å}$ retraction, and h) the final configuration.
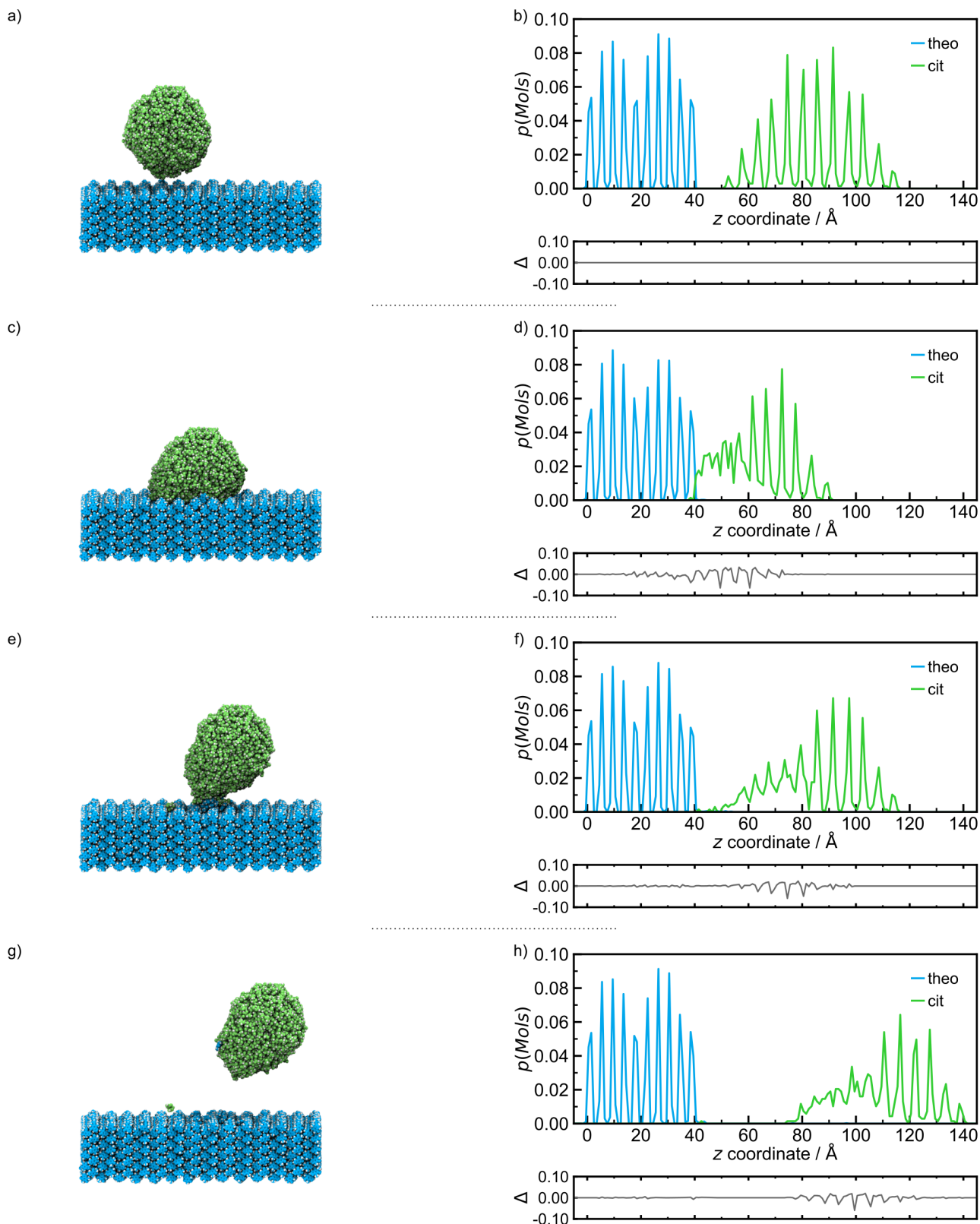
Indentation parameters: $\theta = 45°$, **Indentation speed** $1\,\mathrm{m\,s^{-1}}$
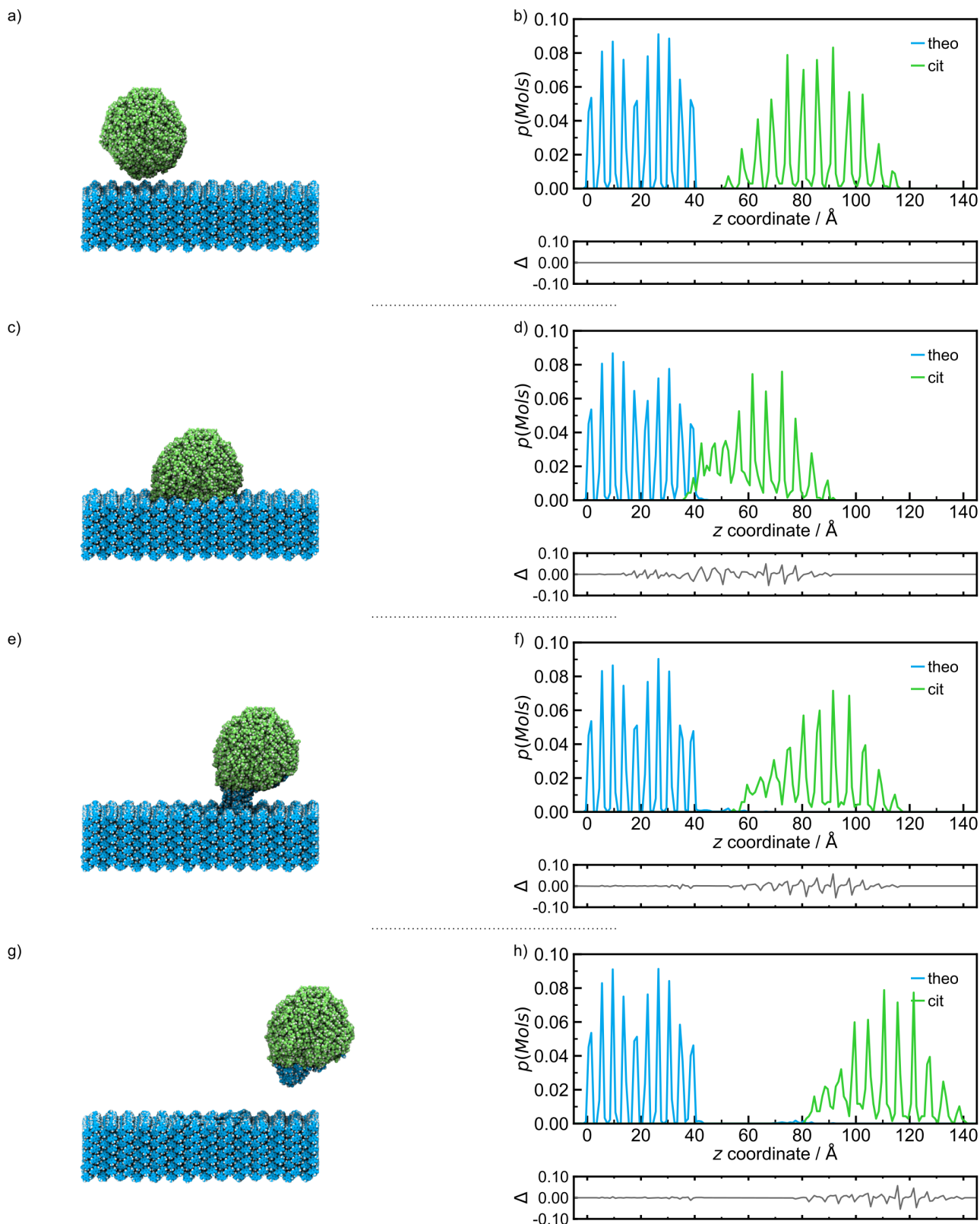

Figure S17 Left: Snapshots of the indentation of **cit** nanoparticle (green) upon the (001) slab of **theo** (blue) where the nanoparticle travels at $1\,\mathrm{m\,s^{-1}}$ and an incident angle of $45°$. The snapshots show a) the initial configuration, c) the point of maximum indentation, e) after retraction of $25\,\mathrm{Å}$, and g) the final configuration after retraction of $50\,\mathrm{Å}$. Hydrogen atoms are rendered in white for aesthetic purposes. Right: Distribution of molecules, as a percentage of the species, of **theo** (blue) and **cit** (green) for b) the initial configuration, d) the point of maximum indentation, f) after $25\,\mathrm{Å}$ retraction, and h) the final configuration.

Indentation parameters: $\theta = 30°$, **Indentation speed** $16\,\mathrm{m\,s^{-1}}$
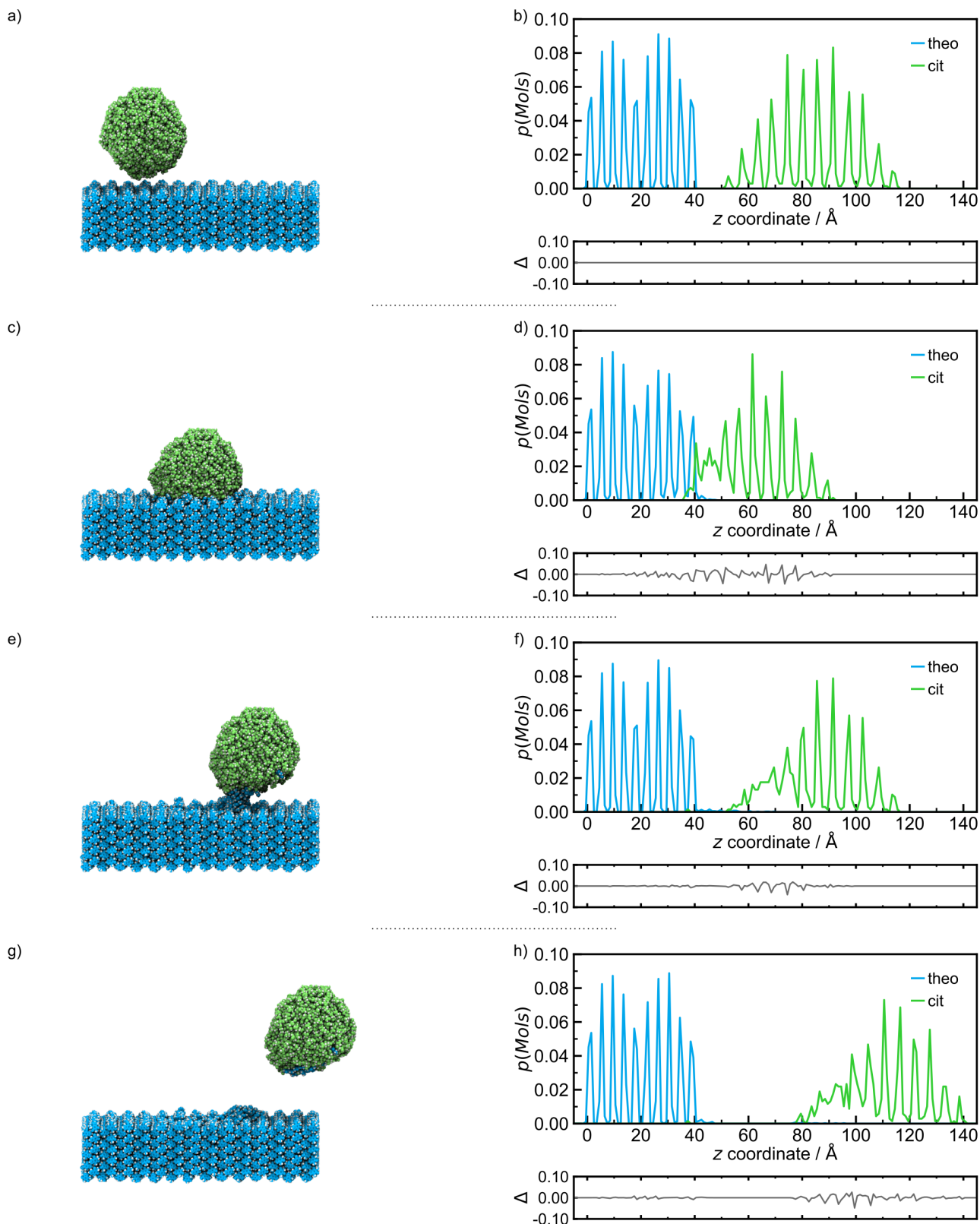

Figure S18 Left: Snapshots of the indentation of **cit** nanoparticle (green) upon the (001) slab of **theo** (blue) where the nanoparticle travels at $16\,\mathrm{m\,s^{-1}}$ and an incident angle of $30°$. The snapshots show a) the initial configuration, c) the point of maximum indentation, e) after retraction of $25\,\text{Å}$, and g) the final configuration after retraction of $50\,\text{Å}$. Hydrogen atoms are rendered in white for aesthetic purposes. Right: Distribution of molecules, as a percentage of the species, of **theo** (blue) and **cit** (green) for b) the initial configuration, d) the point of maximum indentation, f) after $25\,\text{Å}$ retraction, and h) the final configuration.

Indentation parameters: $\theta = 30°$, **Indentation speed** $8\,\mathrm{m\,s^{-1}}$

Figure S19 Left: Snapshots of the indentation of **cit** nanoparticle (green) upon the (001) slab of **theo** (blue) where the nanoparticle travels at $8\,\mathrm{m\,s^{-1}}$ and an incident angle of $30°$. The snapshots show a) the initial configuration, c) the point of maximum indentation, e) after retraction of $25\,\text{Å}$, and g) the final configuration after retraction of $50\,\text{Å}$. Hydrogen atoms are rendered in white for aesthetic purposes. Right: Distribution of molecules, as a percentage of the species, of **theo** (blue) and **cit** (green) for b) the initial configuration, d) the point of maximum indentation, f) after $25\,\text{Å}$ retraction, and h) the final configuration.
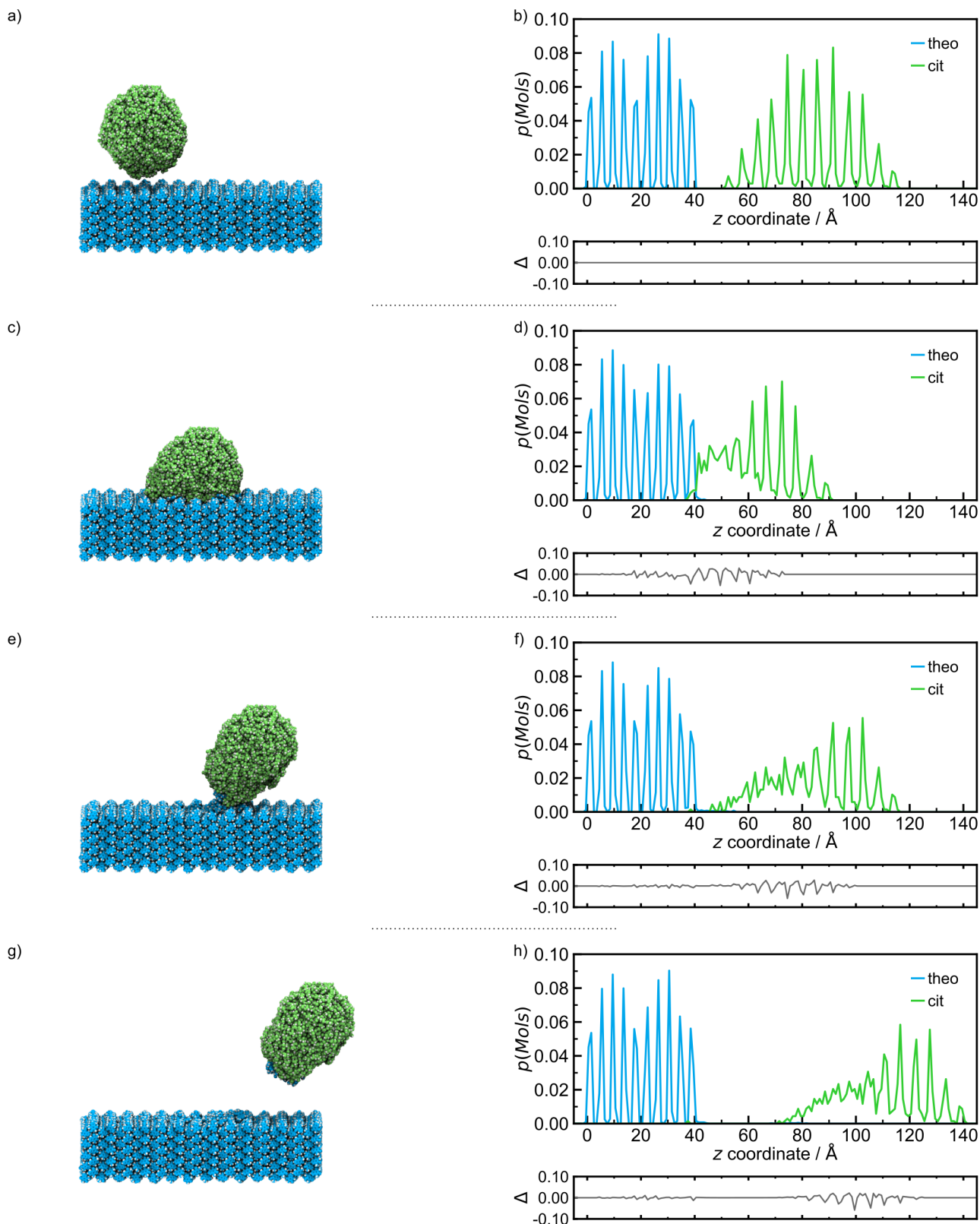
Indentation parameters: $\theta = 30°$, **Indentation speed** $4\,\mathrm{m\,s^{-1}}$

Figure S20 Left: Snapshots of the indentation of **cit** nanoparticle (green) upon the (001) slab of **theo** (blue) where the nanoparticle travels at $4\,\mathrm{m\,s^{-1}}$ and an incident angle of $30°$. The snapshots show a) the initial configuration, c) the point of maximum indentation, e) after retraction of $25\,\text{Å}$, and g) the final configuration after retraction of $50\,\text{Å}$. Hydrogen atoms are rendered in white for aesthetic purposes. Right: Distribution of molecules, as a percentage of the species, of **theo** (blue) and **cit** (green) for b) the initial configuration, d) the point of maximum indentation, f) after $25\,\text{Å}$ retraction, and h) the final configuration.
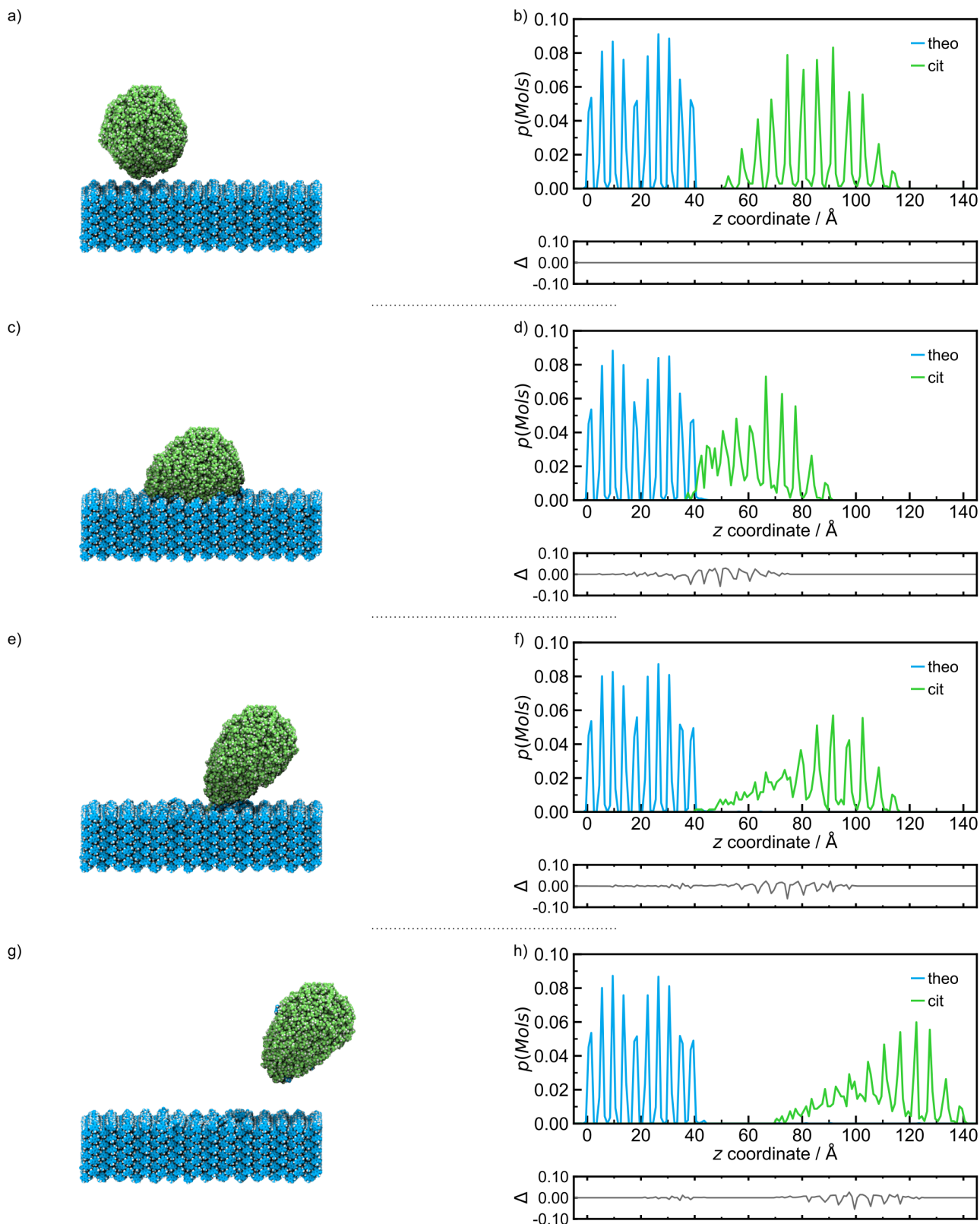
Indentation parameters: $\theta = 30°$, **Indentation speed** $1\,\mathrm{m\,s^{-1}}$
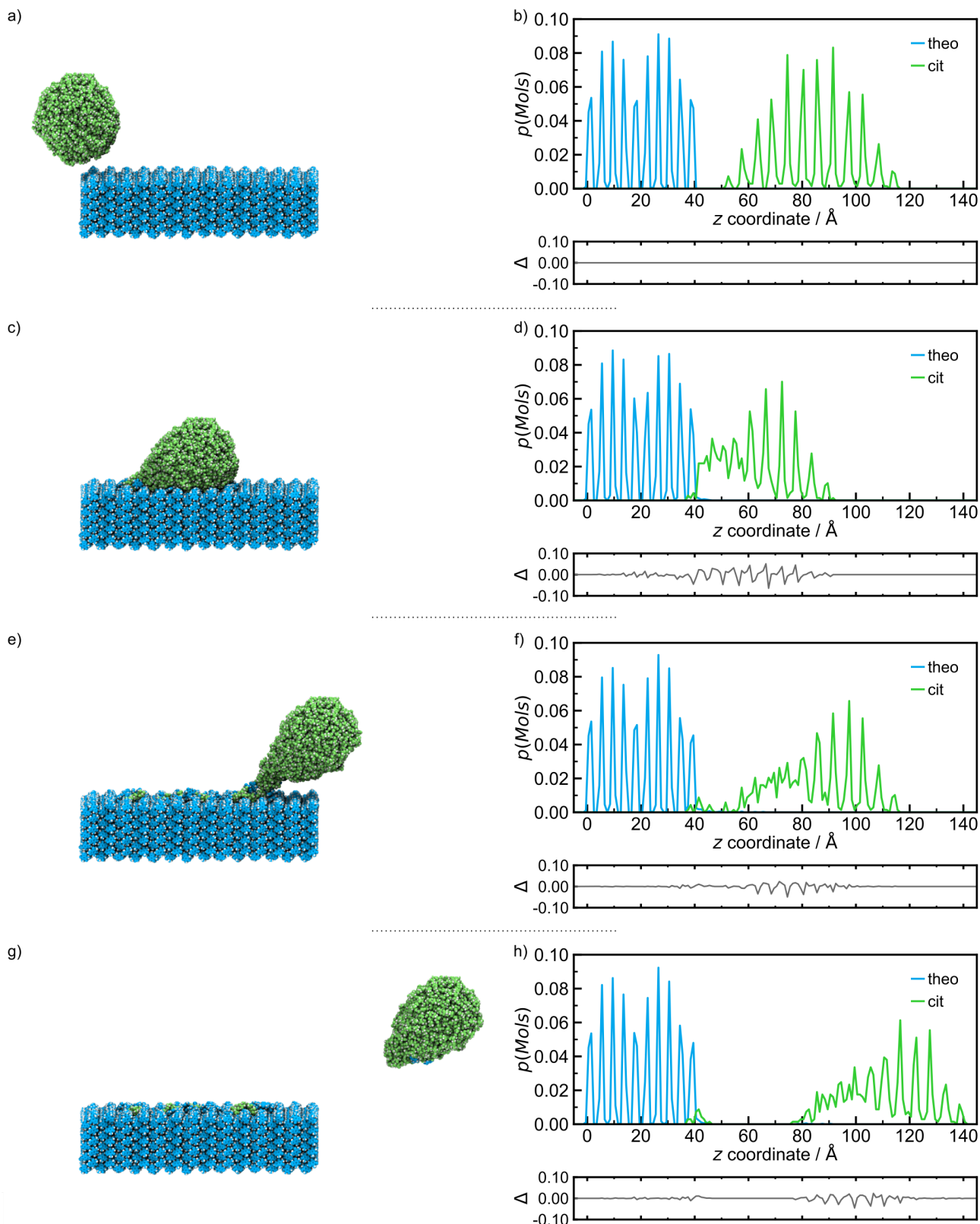

Figure S21 Left: Snapshots of the indentation of **cit** nanoparticle (green) upon the (001) slab of **theo** (blue) where the nanoparticle travels at $1\,\mathrm{m\,s^{-1}}$ and an incident angle of $30°$. The snapshots show a) the initial configuration, c) the point of maximum indentation, e) after retraction of $25\,\text{Å}$, and g) the final configuration after retraction of $50\,\text{Å}$. Hydrogen atoms are rendered in white for aesthetic purposes. Right: Distribution of molecules, as a percentage of the species, of **theo** (blue) and **cit** (green) for b) the initial configuration, d) the point of maximum indentation, f) after $25\,\text{Å}$ retraction, and h) the final configuration.

Indentation parameters: $\theta = 15°$, **Indentation speed** $16\,\mathrm{m\,s^{-1}}$
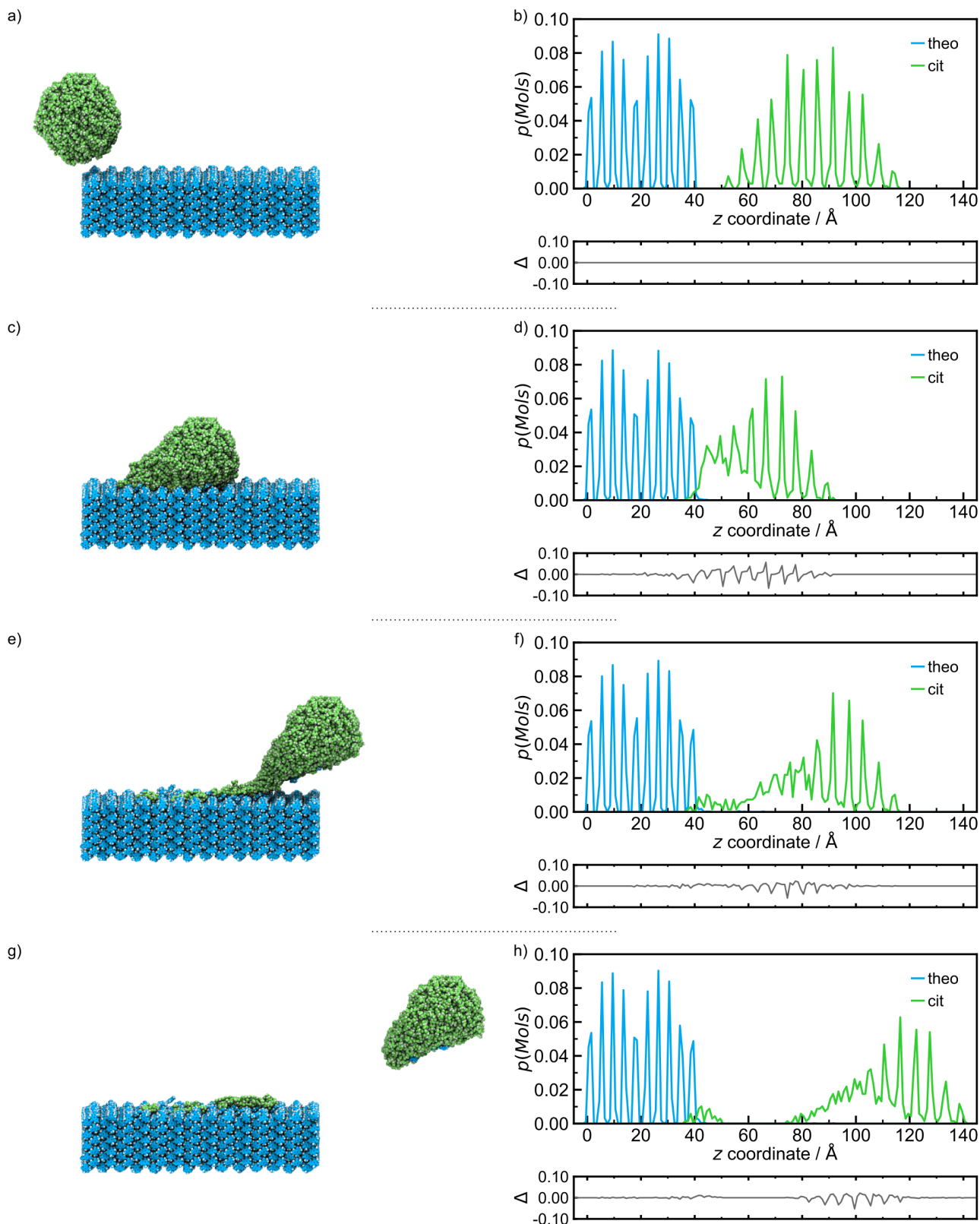

Figure S22 Left: Snapshots of the indentation of **cit** nanoparticle (green) upon the (001) slab of **theo** (blue) where the nanoparticle travels at $16\,\mathrm{m\,s^{-1}}$ and an incident angle of $15°$. The snapshots show a) the initial configuration, c) the point of maximum indentation, e) after retraction of $25\,\text{Å}$, and g) the final configuration after retraction of $50\,\text{Å}$. Hydrogen atoms are rendered in white for aesthetic purposes. Right: Distribution of molecules, as a percentage of the species, of **theo** (blue) and **cit** (green) for b) the initial configuration, d) the point of maximum indentation, f) after $25\,\text{Å}$ retraction, and h) the final configuration.

Indentation parameters: $\theta = 15°$, **Indentation speed** $8\,\mathrm{m\,s^{-1}}$

Figure S23 Left: Snapshots of the indentation of **cit** nanoparticle (green) upon the (001) slab of **theo** (blue) where the nanoparticle travels at $8\,\mathrm{m\,s^{-1}}$ and an incident angle of $15°$. The snapshots show a) the initial configuration, c) the point of maximum indentation, e) after retraction of $25\,\text{Å}$, and g) the final configuration after retraction of $50\,\text{Å}$. Hydrogen atoms are rendered in white for aesthetic purposes. Right: Distribution of molecules, as a percentage of the species, of **theo** (blue) and **cit** (green) for b) the initial configuration, d) the point of maximum indentation, f) after $25\,\text{Å}$ retraction, and h) the final configuration.

Indentation parameters: $\theta = 15°$, **Indentation speed** $4\,\mathrm{m\,s^{-1}}$

Figure S24 Left: Snapshots of the indentation of **cit** nanoparticle (green) upon the (001) slab of **theo** (blue) where the nanoparticle travels at $4\,\mathrm{m\,s^{-1}}$ and an incident angle of $15°$. The snapshots show a) the initial configuration, c) the point of maximum indentation, e) after retraction of $25\,\text{Å}$, and g) the final configuration after retraction of $50\,\text{Å}$. Hydrogen atoms are rendered in white for aesthetic purposes. Right: Distribution of molecules, as a percentage of the species, of **theo** (blue) and **cit** (green) for b) the initial configuration, d) the point of maximum indentation, f) after $25\,\text{Å}$ retraction, and h) the final configuration.
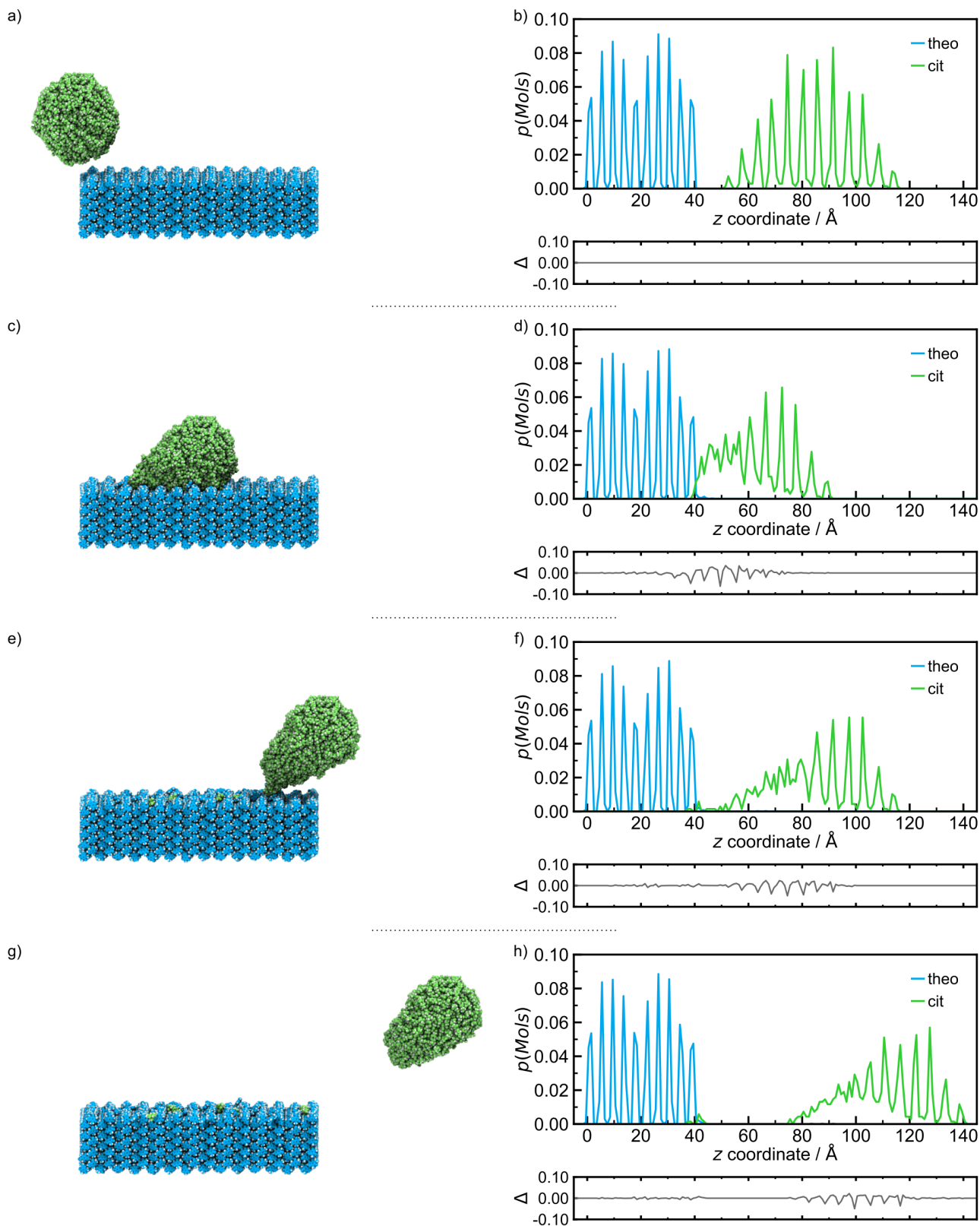
Indentation parameters: $\theta = 15°$, **Indentation speed** $1\,\mathrm{m\,s^{-1}}$

Figure S25 Left: Snapshots of the indentation of **cit** nanoparticle (green) upon the (001) slab of **theo** (blue) where the nanoparticle travels at $1\,\mathrm{m\,s^{-1}}$ and an incident angle of $15°$. The snapshots show a) the initial configuration, c) the point of maximum indentation, e) after retraction of $25\,\text{Å}$, and g) the final configuration after retraction of $50\,\text{Å}$. Hydrogen atoms are rendered in white for aesthetic purposes. Right: Distribution of molecules, as a percentage of the species, of **theo** (blue) and **cit** (green) for b) the initial configuration, d) the point of maximum indentation, f) after $25\,\text{Å}$ retraction, and h) the final configuration.
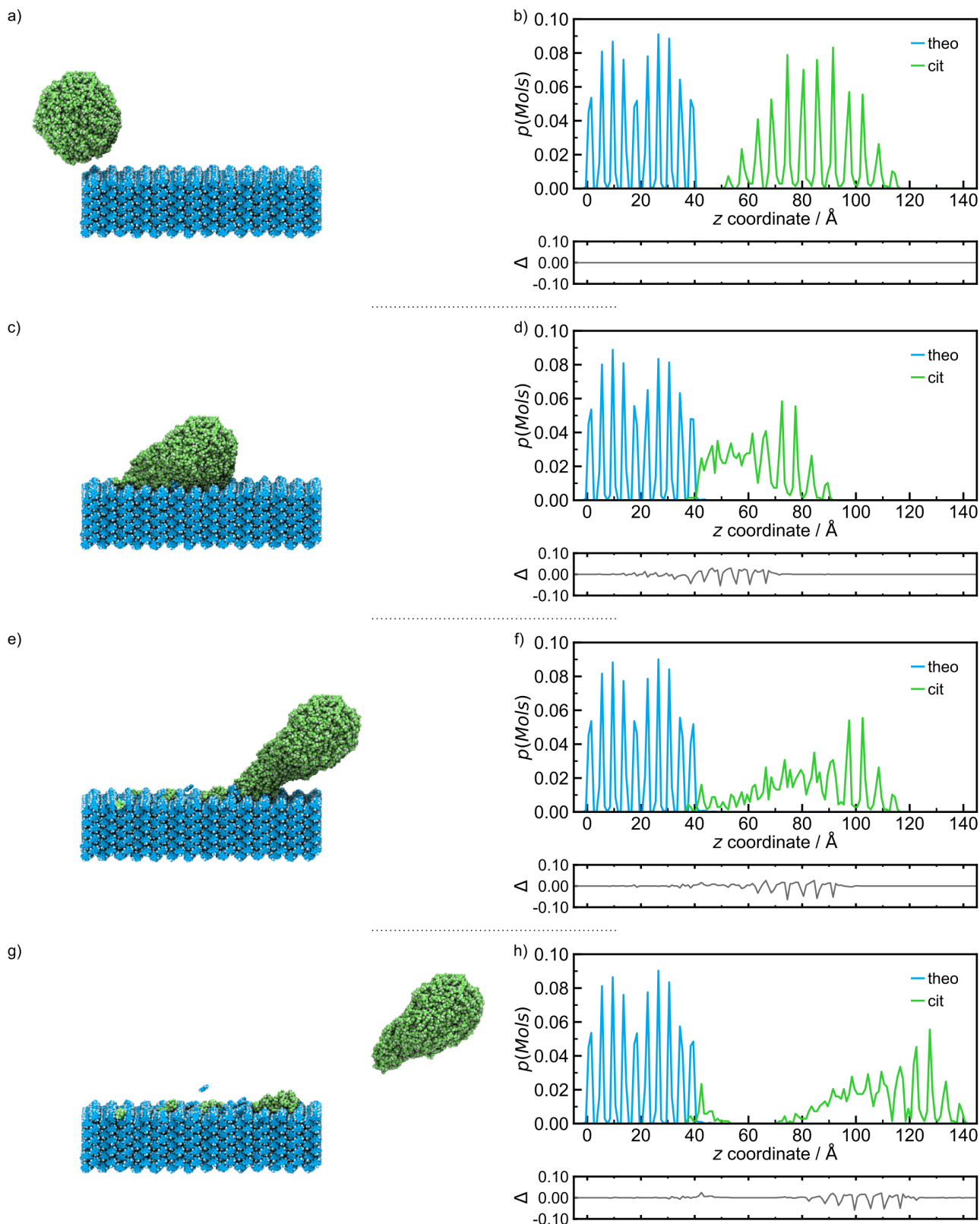
S3 Connective neck analysis

In the majority of cases in this study a connective neck between the nanoparticle and slab forms during the retraction process. To estimate the length of the connective neck l_{cn} we looked at the z separation between the sections of the **cit** and **theo** whose trajectories were fixed during the simulation. After the nanoparticle has been retracted by $20\,\text{Å}$ the z coordinates of the nanoparticle identical to when it first touches the surface, due to the initial $5\,\text{Å}$ separation. Each simulation trajectory was then monitored to find the last frame in which a connective neck is observed. The distance (d) travelled is then calculated as;

$$d = v_z \cdot t_{cn}$$

where v_z is the z component of velocity in $\text{Å}\,\text{fs}^{-1}$ and t_{cn} is the number of simulation steps taken to break the connective neck multiplied by the time step of integration (1 fs). The angle of incidence θ must also be considered when estimating the connective neck length. As the x component of the velocity remains unchanged during the retraction the angle of retraction is equal to the angle of incidence. Therefore, l_{cn} can be estimated as;

$$l_{cn} = d \sin(\theta)$$

A graphical description of this calculation is shown in Figure S26 and the values of the estimated connective lengths are given in Table S5
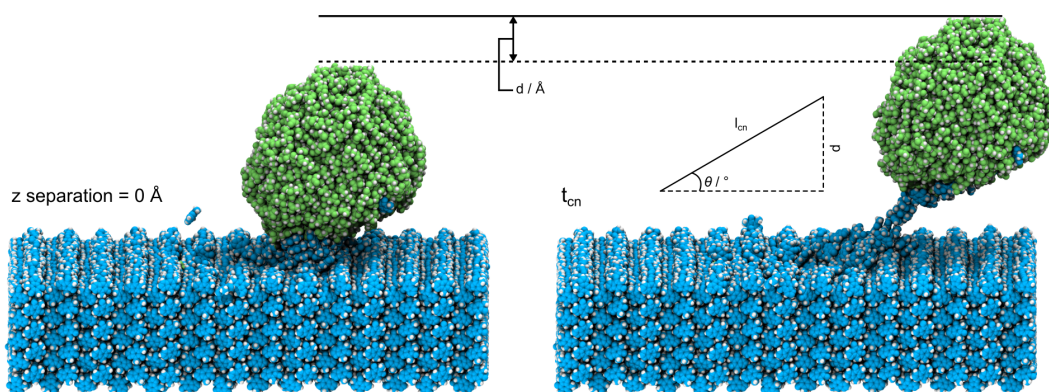
Figure S26 Scheme depicting how the connective neck length was estimated in this study. Left: Snapshot of the retraction of **cit** nanoparticle (green) from the slab of **theo** (blue) at a given θ ($\theta = 30°$ in this case) where the nanoparticle has been retracted by $20\,\text{Å}$ and is considered to be at the point where the separation of the two objects is equal to zero. Right: Snapshots of the system at t_{cn} where a connective neck is still visible in the simulation. Solid and dotted horizontal black lines show how the distance travelled d is calculated and the inset triangle show the relation ship between θ, d, and l_{cn}. Hydrogen atoms are rendered in white for aesthetic purposes.

Table S4 Time during which the connective neck exists between **cit** and **theo** during simulated indentations for a range of indentation speeds ($16\,\text{m s}^{-1}$ to $1\,\text{m s}^{-1}$) and angles ($\theta = 90°$ to $15°$).

v / m s^{-1}	θ / °					
	90	75	60	45	30	15
	t_{cn} / ns					
16	-	0.05	0.02	-	0.19	0.20
8	-	0.11	0.11	0.25	0.46	0.56
4	0.16	0.30	0.32	0.49	0.96	1.16
1	1.77	2.05	3.12	2.57	3.65	6.17

Table S5 Estimated connective neck lengths for necks formed between **cit** and **theo** during simulated indentations for a range of indentation speeds ($16\,\mathrm{m\,s^{-1}}$ to $1\,\mathrm{m\,s^{-1}}$) and angles ($\theta = 90^\circ$ to 15°).

	θ / °					
v / $\mathrm{m\,s^{-1}}$	90	75	60	45	30	15
	l_{cn} / nm					
16	-	0.81	0.31	-	3.06	3.21
8	-	0.88	0.88	2.01	3.68	4.56
4	0.64	1.19	1.28	1.95	3.82	4.64
1	1.77	2.00	3.12	2.57	3.64	6.18

S4 Sphericity analysis

Using the Ovito[19] program, all atoms whose z coordinate was above 55 Å were selected and used to construct a surface mesh of the nanoparticle after the simulated indentation. For the initial configuration, all atoms of **cit** were selected to construct the mesh as no mixing had occurred. The probe radius was set at 3 Å and a surface smoothing level of 10 applied. The program then provides values for the area (S) of, and volume (V) contained within the constructed surface. Then the radius (r_{ideal}) and surface area (S_{ideal}) of the perfect sphere are determined by;

$$r_{ideal} = \left(\frac{3V}{4\pi}\right)^{\frac{1}{3}}$$

$$S_{ideal} = 4\pi r_{ideal}^2$$

The sphericity is then calculated as;

$$\Psi = \frac{S_{ideal}}{S}$$

With Ψ of the initial configuration used as a reference $\Delta\%\Psi$ was calculated for each indentation. All values of the measured and calculated parameters used analyse the sphericity of the nanoparticle are given in Table S6

Table S6 Surface areas (S) and volumes (V) of the **cit** nanoparticle determined by a surface mesh analysis with the ideal radii (r_{ideal}) and surface areas (S_{ideal}) using to calculate the sphericity (Ψ) and percentage change in sphericity ($\Delta\%\Psi$) after simulated indentations over a range of indentation speeds ($16\,\mathrm{m\,s^{-1}}$ to $1\,\mathrm{m\,s^{-1}}$) and angles ($\theta = 90°$ to $15°$).

| θ / °	v / $\mathrm{m\,s^{-1}}$	S / Å^2	V / Å^3	r_{ideal} / Å	S_{ideal} / Å^2	Ψ	$\Delta\%\Psi$
Initial	Initial	13955.8	132057.0	31.59	12540.80	0.899	0.0
90	16	14216.0	133063.0	31.67	12604.40	0.887	-1.3
	8	14328.3	135189.0	31.84	12738.31	0.889	-1.1
	4	14297.2	132531.0	31.63	12570.79	0.879	-2.2
	1	14185.7	132612.0	31.64	12575.91	0.887	-1.3
75	16	14251.9	133518.0	31.71	12633.12	0.886	-1.4
	8	14238.1	132736.0	31.65	12583.75	0.884	-1.6
	4	14199.8	132439.0	31.62	12564.97	0.885	-1.5
	1	14124.9	132640.0	31.64	12577.68	0.890	-0.9
60	16	14248.0	133783.0	31.73	12649.83	0.888	-1.2
	8	14347.2	133721.0	31.72	12645.92	0.881	-1.9
	4	14442.0	133775.0	31.73	12649.33	0.876	-2.5
	1	14643.4	131906.0	31.58	12531.23	0.856	-4.8
45	16	14238.6	132765.0	31.65	12585.58	0.884	-1.6
	8	14439.9	134059.0	31.75	12667.22	0.877	-2.4
	4	14290.1	133153.0	31.68	12610.09	0.882	-1.8
	1	14166.1	131260.0	31.56	12490.29	0.882	-1.9
30	16	15084.7	140504.0	32.25	13070.03	0.866	-3.6
	8	14557.0	134808.0	31.81	12714.36	0.873	-2.8
	4	14729.5	134102.0	31.75	12669.93	0.860	-4.3
	1	14396.8	131802.0	31.57	12524.65	0.870	-3.2
15	16	14436.9	129328.0	31.37	12367.42	0.857	-4.7
	8	14246.1	124329.0	30.96	12046.64	0.846	-5.9
	4	14391.8	130477.0	31.46	12440.57	0.864	-3.8
	1	14253.3	119510.0	30.56	11733.30	0.823	-8.4

S5 Force development analysis

Following previous studies of indentations[20] we analysed the development of the force in z throughout the indentation process. To achieve this atomic forces for the 392 **theo** and 115 **cit** molecules whose trajectories were fixed to control the simulations were collected as two separate outputs from the LAMMPS MD simulation runs. Then, for each species, the force component along the direction of indentation (z) was extracted for each frame of the trajectory to be plotted against the separation of the two species in z. We track the z separation through in a similar fashion as described in Section S4, i.e. by using the z component of velocity and product of the number of simulation steps and the integration time step, taking care to account for of the change in direction of the velocity after the point of maximum indentation. The simulated indentations performed required a wide range of simulation times (0.5 ns to 29 ns) as a result of the change in incident angle and speed. Therefore, the number of data points for each simulation varied. To account for this we applied a moving average to the raw data, relative to the indentation velocity. Given the low number of data points when the indentation speed was $16 \, \mathrm{m \, s^{-1}}$, the size of the average was set to 1 meaning that no averaging was applied. Then for subsequent speeds the moving average size was inversely proportional to the reduction in speed. Specifically, the size of moving averages for $8 \, \mathrm{m \, s^{-1}}$, $4 \, \mathrm{m \, s^{-1}}$, and $1 \, \mathrm{m \, s^{-1}}$ were 2, 4, and 16, respectively. The extra simulation time due to the reduction in θ was not incorporated into the moving averages amount of simulated time did not increase by an integer factor when $\theta = 75°$, $60°$, or $45°$ relative to when $\theta = 90°$. In all cases the direction of the force development is opposite for **cit** and **theo** (Figures S27-S32) but the magnitude of forces for **theo** is significantly lower than for **cit**. We ascribe this to the unequal number of molecules of each species whose trajectories were controlled during the indentation, with the number of **theo** molecules being a factor or 3.4 greater than for **cit**. Coincidentally individual molecules of both species are comprised of 21 atoms each. Focusing on the force development for **cit**, as v is decreased a reduction in the magnitude of the force is observed which is most evident when $\theta = 90°$ (Figure S27) but less so at lower θ values. There is also a reduction in force as θ decreases which is most noticeable when comparing the force development plots for $\theta = 30°$ (Figure S31) and $\theta = 15°$ (Figure S32) with that of $\theta = 90°$ (Figure S27). Interestingly, the maximum force observed in this study is approximately 10 pN with is an order of magnitude lower than that observed previously,[20c] but within the force range said to be expected for hydrogen bonded systems.[21]
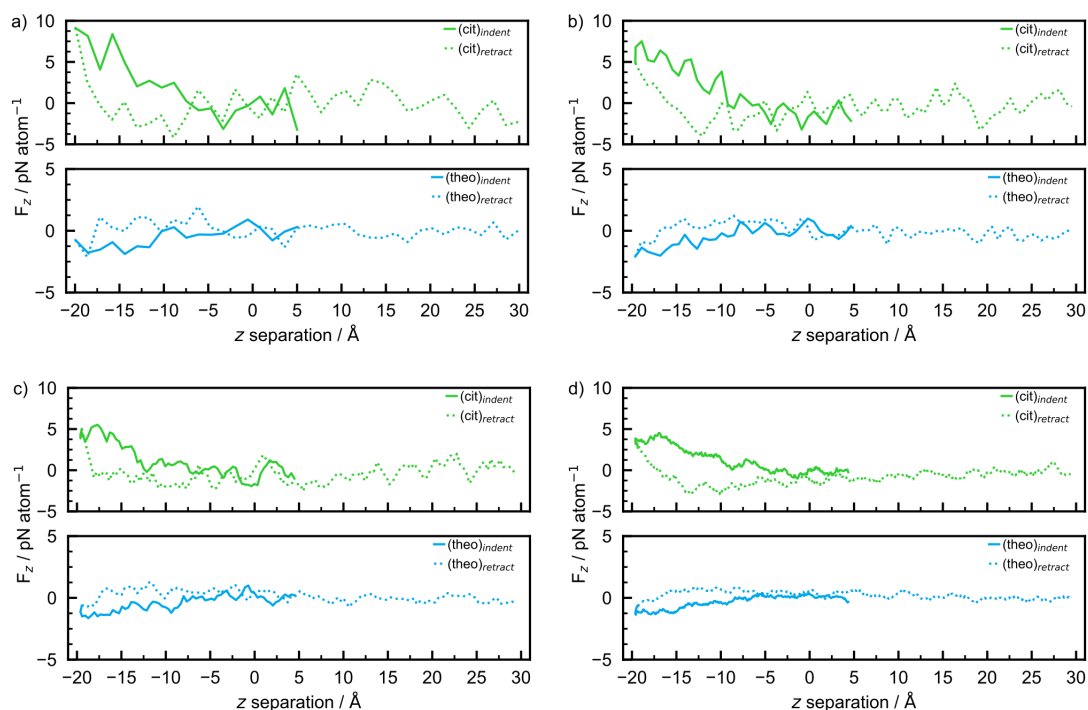
Indentation parameters: $\theta = 90°$
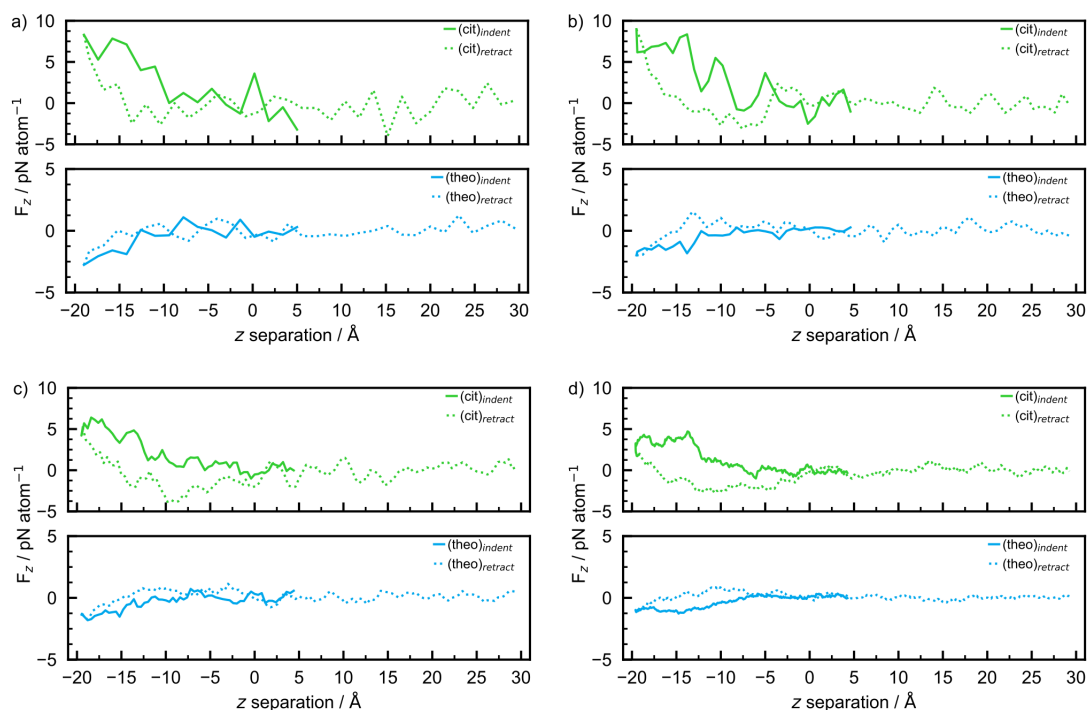
Figure S27 Development of the force in z experienced by the fixed trajectory sections of **cit** (green, top panel) and **theo** (blue, bottom panel) during a simulated indentation with $\theta = 90°$ and Indentation speed a) $16\,\mathrm{m\,s^{-1}}$, b) $8\,\mathrm{m\,s^{-1}}$, c) $4\,\mathrm{m\,s^{-1}}$, and d) $1\,\mathrm{m\,s^{-1}}$. Solid lines representation the indentation stage while dotted lines represent the retraction stage of the simulation.

Indentation parameters: $\theta = 75°$
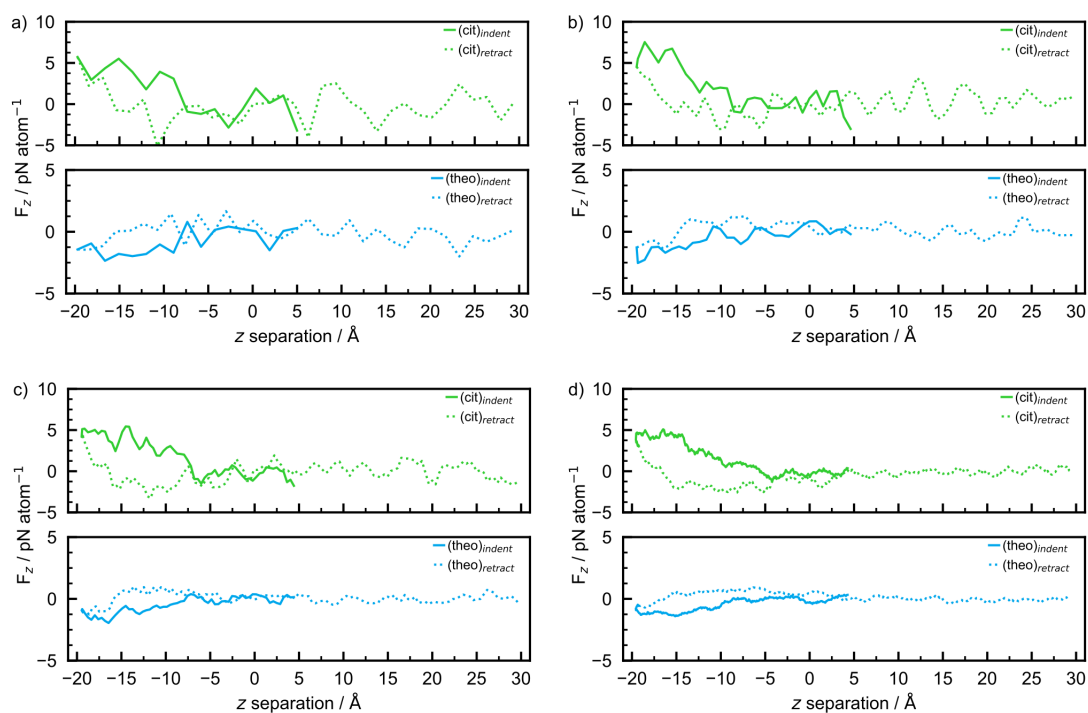
Figure S28 Development of the force in z experienced by the fixed trajectory sections of **cit** (green, top panel) and **theo** (blue, bottom panel) during a simulated indentation with $\theta = 75°$ and Indentation speed a) $16\,\mathrm{m\,s^{-1}}$, b) $8\,\mathrm{m\,s^{-1}}$, c) $4\,\mathrm{m\,s^{-1}}$, and d) $1\,\mathrm{m\,s^{-1}}$. Solid lines representation the indentation stage while dotted lines represent the retraction stage of the simulation.
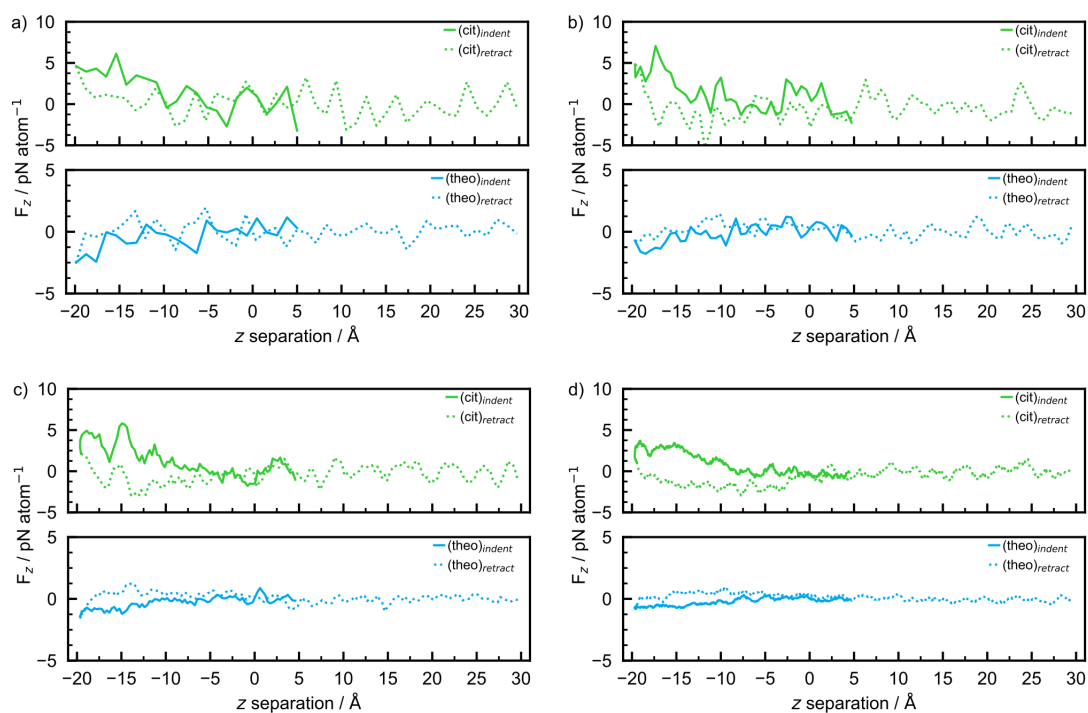
Indentation parameters: $\theta = 60°$

Figure S29 Development of the force in z experienced by the fixed trajectory sections of **cit** (green, top panel) and **theo** (blue, bottom panel) during a simulated indentation with $\theta = 60°$ and Indentation speed a) $16\,\mathrm{m\,s^{-1}}$, b) $8\,\mathrm{m\,s^{-1}}$, c) $4\,\mathrm{m\,s^{-1}}$, and d) $1\,\mathrm{m\,s^{-1}}$. Solid lines representation the indentation stage while dotted lines represent the retraction stage of the simulation.

Indentation parameters: $\theta = 45°$

Figure S30 Development of the force in z experienced by the fixed trajectory sections of **cit** (green, top panel) and **theo** (blue, bottom panel) during a simulated indentation with $\theta = 45°$ and Indentation speed a) $16\,\mathrm{m\,s^{-1}}$, b) $8\,\mathrm{m\,s^{-1}}$, c) $4\,\mathrm{m\,s^{-1}}$, and d) $1\,\mathrm{m\,s^{-1}}$. Solid lines representation the indentation stage while dotted lines represent the retraction stage of the simulation.
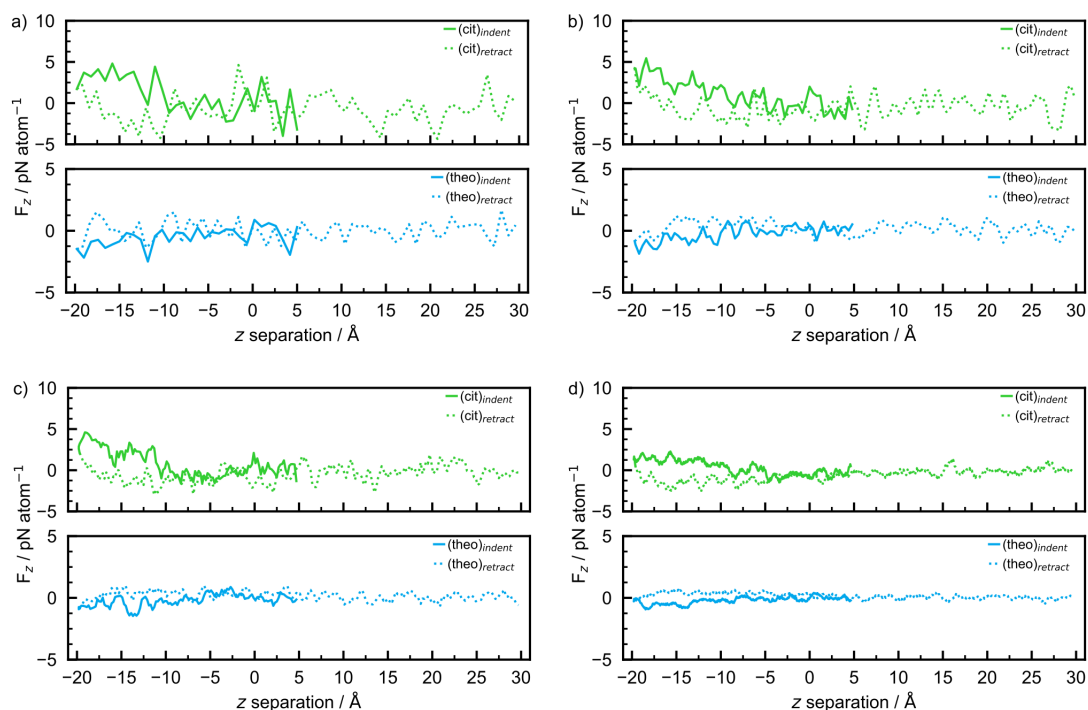
Indentation parameters: $\theta = 30°$

Figure S31 Development of the force in z experienced by the fixed trajectory sections of **cit** (green, top panel) and **theo** (blue, bottom panel) during a simulated indentation with $\theta = 30°$ and Indentation speed a) $16\,\mathrm{m\,s^{-1}}$, b) $8\,\mathrm{m\,s^{-1}}$, c) $4\,\mathrm{m\,s^{-1}}$, and d) $1\,\mathrm{m\,s^{-1}}$. Solid lines representation the indentation stage while dotted lines represent the retraction stage of the simulation.
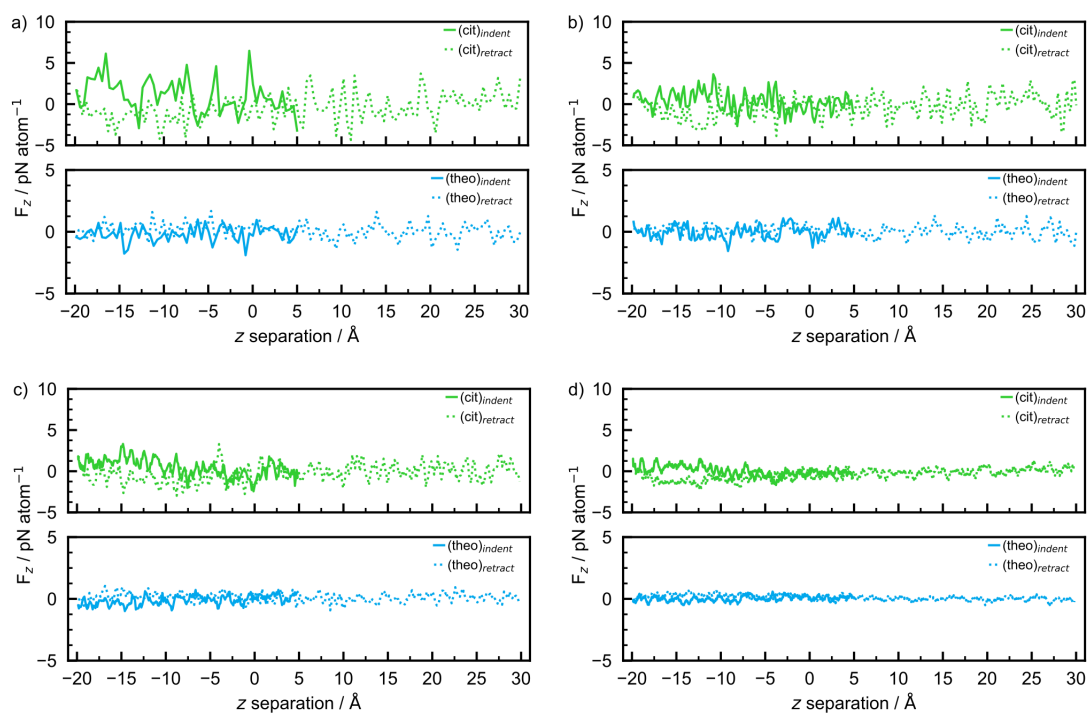
Indentation parameters: $\theta = 15°$

Figure S32 Development of the force in z experienced by the fixed trajectory sections of **cit** (green, top panel) and **theo** (blue, bottom panel) during a simulated indentation with $\theta = 15°$ and Indentation speed a) $16\,\mathrm{m\,s^{-1}}$, b) $8\,\mathrm{m\,s^{-1}}$, c) $4\,\mathrm{m\,s^{-1}}$, and d) $1\,\mathrm{m\,s^{-1}}$. Solid lines representation the indentation stage while dotted lines represent the retraction stage of the simulation.

S6 Description of videos

A folder of supplementary videos is provided with this manuscript. The folder contains a rendered trajectory for each of the simulated indentations presented in this work. The filenames are *indent_cit-theo_MMdeg-NNms.mp4* where MM is the incident angle of the **cit** nanoparticle and NN is the indentation speed. Due to the large discrepancy in simulation time across the indentations videos were rendered at 24 fps, 18 fps, 12 fps, and 6 fps for indentation speeds of $1 \, \mathrm{m \, s^{-1}}$, $4 \, \mathrm{m \, s^{-1}}$, $8 \, \mathrm{m \, s^{-1}}$, and $16 \, \mathrm{m \, s^{-1}}$, respectively.

References

[1] S. Plimpton, *J. Comput. Phys.*, 1995, **117**, 1 – 19.

[2] (*a*) W. L. Jorgensen and J. Tirado-Rives, *J. Am. Chem. Soc.*, 1988, **110**, 1657–1666; (*b*) W. L. Jorgensen, D. S. Maxwell and J. Tirado-Rives, *J. Am. Chem. Soc.*, 1996, **118**, 11225–11236.

[3] J. E. Lennard-Jones, *Proc. Phys. Soc.*, 1931, **43**, 461.

[4] S. L. Mayo, B. D. Olafson and W. A. Goddard, *J. Phys. Chem.*, 1990, **94**, 8897–8909.

[5] R. Hockney and J. Eastwood, *Computer Simulation Using Particles*, Taylor & Francis, New York, 1998.

[6] W. Humphrey, A. Dalke and K. Schulten, *J. Mol. Graphics*, 1996, **14**, 33–38.

[7] J. E. Stone, *M.Sc. thesis*, University of Missouri-Rolla, MO, USA, 1996.

[8] S. J. Clark, M. D. Segall, C. J. Pickard, P. J. Hasnip, M. I. J. Probert, K. Refson and M. C. Payne, *Z. Kristallogr. Cryst. Mater.*, 2005, **220**, 567–570.

[9] C. R. Groom, I. J. Bruno, M. P. Lightfoot and S. C. Ward, *Acta Crystallogr., Sect. B: Struct. Sci., Cryst. Eng. Mater.*, 2016, **72**, 171–179.

[10] J. P. Glusker, J. A. Minkin and A. L. Patterson, *Acta Crystallogr., Sect. B: Struct. Sci., Cryst. Eng. Mater.*, 1969, **25**, 1066–1072.

[11] Y. Ebisuzaki, P. D. Boyle and J. A. Smith, *Acta Crystallogr., Sect. C: Struct. Chem.*, 1997, **53**, 777–779.

[12] T. Björkman, *Comput. Phys. Commun.*, 2011, **182**, 1183 – 1186.

[13] J. P. Perdew, K. Burke and M. Ernzerhof, *Phys. Rev. Lett.*, 1996, **77**, 3865–3868.

[14] S. Grimme, J. Antony, S. Ehrlich and H. Krieg, *J. Chem. Phys.*, 2010, **132**, 154104.

[15] F. L. Hirshfeld, *Theor. Chim. Acta*, 1977, **44**, 129–138.

[16] G. Van Rossum and F. L. Drake, *Python 3 Reference Manual*, CreateSpace, Scotts Valley, CA, 2009.

[17] C. R. Harris, K. J. Millman, S. J. van der Walt, R. Gommers, P. Virtanen, D. Cournapeau, E. Wieser, J. Taylor, S. Berg, N. J. Smith, R. Kern, M. Picus, S. Hoyer, M. H. van Kerkwijk, M. Brett, A. Haldane, J. F. del Río, M. Wiebe, P. Peterson, P. Gérard-Marchant, K. Sheppard, T. Reddy, W. Weckesser, H. Abbasi, C. Gohlke and T. E. Oliphant, *Nature*, 2020, **585**, 357–362.

[18] J. D. Hunter, *Comput. Sci. Eng.*, 2007, **9**, 90–95.

[19] A. Stukowski, *Modell. Simul. Mater. Sci. Eng.*, 2010, **18**, 015012.

[20] (*a*) K. Komvopoulos and W. Yan, *J. Appl. Phys.*, 1997, **82**, 4823–4830; (*b*) C. Ruestes, E. Bringa, Y. Gao and H. Urbassek, in *Molecular Dynamics Modeling of Nanoindentation*, John Wiley & Sons, Ltd, 2017, ch. 14, pp. 313–345; (*c*) M. Ferguson, M. S. Moyano, G. A. Tribello, D. E. Crawford, E. M. Bringa, S. L. James, J. Kohanoff and M. G. Del Pópolo, *Chem. Sci.*, 2019, **10**, 2924–2929.

[21] J. Ribas-Arino and D. Marx, *Chem. Rev.*, 2012, **112**, 5412–5487.